CDF Note 10609

# Combination of CDF's Searches for the Standard Model Higgs boson with up to 8.2 fb$^{-1}$ of Data

The CDF Higgs Discovery Group

*for the CDF Collaboration*

*October 26, 2011*

We combine results from CDF's direct searches for the standard model (SM) Higgs boson ($H$) in $p\bar{p}$ collisions at the Fermilab Tevatron at $\sqrt{s} = 1.96$ TeV. Compared to the previous Tevatron Higgs search combination more data have been added, additional new channels have been incorporated, and some previously used channels have been reanalyzed to gain sensitivity. We use the latest parton distribution functions and $gg \to H$ theoretical cross sections when comparing our limits to the SM predictions. With up to 8.2 fb$^{-1}$ of data, the 95% C.L. upper limits on Higgs boson production are 1.55 and 0.75 times the values of the SM cross section for Higgs boson masses of $m_H$ =115 GeV/$c^2$ and 165 GeV/$c^2$, respectively. We exclude, at the 95% C.L., a new and larger region at high mass between $156.5 < m_H < 173.7$ GeV/$c^2$.

*Preliminary Results*

## I. INTRODUCTION

The search for a mechanism for electroweak symmetry breaking, and in particular for a standard model (SM) Higgs boson, has been a major goal of particle physics for many years, and is a central part of the Fermilab Tevatron physics program. We have updated our searches for the SM Higgs boson, and a combination of these searches with those of D0 [1] is available in Ref. [2]. direct searches for the SM Higgs boson. The new searches include more data, the inclusion of additional channels, and improved analysis techniques compared to previous analyses. The sensitivities of these new combinations significantly exceed those of previous combinations [3, 4].

In this note, we combine the most recent results of all such searches in $p\bar{p}$ collisions at $\sqrt{s} = 1.96$ TeV. The analyses combined here seek signals of Higgs bosons produced in association with vector bosons ($q\bar{q} \to W/ZH$), through gluon-gluon fusion ($gg \to H$), and through vector boson fusion (VBF) ($q\bar{q} \to q'\bar{q}'H$) corresponding to integrated luminosities up to 8.2 fb$^{-1}$. In order to report an integrated luminosity corresponding to the data sample used to make our results, we average together the contributing searches' luminosities in a way that represents their contributions to the final results. A search with a low sensitivity contributes less to the average than searches with higher sensitivity. The overall sensitivity-weighted luminosities at low ($< 135$ GeV/$c^2$) and high mass ($> 135$ GeV/$c^2$) are 7.5 fb$^{-1}$ and 8.2 fb$^{-1}$, respectively. The Higgs boson decay modes studied are $H \to b\bar{b}$, $H \to W^+W^-$, $H \to Z^\circ Z^\circ$, $H \to \tau^+\tau^-$ and $H \to \gamma\gamma$.

To simplify the combination, the searches are separated into 71 mutually exclusive final states, which are listed in Table II, and which are referred to as "analysis sub-channels" in this note. The selection procedures for each analysis are detailed in Refs. [5] through [17], and are briefly described below.

## II. SUMMARY OF INCLUDED ANALYSES

For the case of $WH \to \ell\nu b\bar{b}$, an isolated lepton ($\ell$ = electron or muon) and two jets are required, with one or more $b$-tagged jets, i.e., identified as containing a weakly-decaying $B$ hadron. Selected events must also display a significant imbalance in transverse momentum (referred to as missing transverse energy or $\not\!\!E_T$). Events with more than one isolated lepton are vetoed.

For the $WH \to \ell\nu b\bar{b}$ analyses, events are analyzed in two and three jet sub-channels separately, and in each of these samples the events are grouped into various lepton and $b$-tag categories. Events are broken into separate analysis categories based on the quality of the identified lepton. Separate categories are used for events with a high quality muon or central electron candidate, an isolated track or identified loose muon in the extended muon coverage, a forward electron candidate, and a loose central electron or isolated track candidate. The final two lepton categories on this list, which provide some acceptance for lower quality electrons and single prong tau decays, are used only in the case of two jet events. Within the lepton categories there are four $b$-tagging categories considered for two jet events: two tight $b$-tags (TDT), one tight $b$-tag and one loose $b$-tag (LDT), one tight $b$-tag and one looser $b$-tag (LDTX), and a single, tight, $b$-tag (ST). For three jet events there is no LDTX tagging category and the corresponding events are included within the ST category. In the case of the two jet events, a Bayesian neural network discriminant is trained at each $m_H$ within the test range for each of the specific categories (defined by lepton type, $b$-tagging type, and number of jets), while matrix element (ME) discriminants are used for each three jet event category.

For the $ZH \to \nu\bar{\nu}b\bar{b}$ analyses, the selection is similar to the $WH$ selection, except all events with isolated leptons are vetoed and stronger multijet background suppression techniques are applied. The analyses use a track-based missing transverse momentum calculation as a discriminant against false $\not\!\!E_T$. In addition, we use a neural network to further discriminate against the multi-jet background before $b$-tagging. There is a sizable fraction of the $WH \to \ell\nu b\bar{b}$ signal in which the lepton is undetected that is selected in the $ZH \to \nu\bar{\nu}b\bar{b}$ samples, so these analyses are also referred to as $VH \to \not\!\!E_T b\bar{b}$. Our analysis uses three non-overlapping categories of $b$-tagged events (TDT, LDT and ST where the LDTX events defined for the $WH \to \ell\nu b\bar{b}$ channels are in this case included as part of the ST channel). We use neural-network outputs for the final discriminating variables.

The $ZH \to \ell^+\ell^- b\bar{b}$ analyses require two isolated leptons and at least two jets. We separate events into single tag (ST), double tag (TDT) and loose double tag (LDT) samples. These analyses use neural networks to select loose dielectron and dimuon candidates. The jet energies are correted for $\not\!\!E_T$ using a neural network approach. We use a

multi-layer discriminant based on neural networks where two expert discriminant functions are used to define three separate regions of the final discriminant function.

For the $H \to W^+W^-$ analyses, signal events are characterized by large $\not\!\!E_T$ and two opposite-signed, isolated leptons. The presence of neutrinos in the final state prevents the accurate reconstruction of the candidate Higgs boson mass. The $H \to W^+W^-$ events are separated in five non-overlapping samples, split based on "high $s/b$" and "low $s/b$" categories defined by lepton types and the number of reconstructed jets: 0, 1, or 2+ jets. The sample with two or more jets is not split into low $s/b$ and high $s/b$ lepton categories due to the smaller statistics in this channel. A sixth channel is the low dilepton mass ($m_{\ell^+\ell^-}$) channel, which accepts events with $m_{\ell^+\ell^-} < 16$ GeV. A new feature of the analysis is the ability to recover of events with lepton pairs that lie within each other's isolation cones. This feature leads to a significant increase in sensitivity from the low $m_{\ell^+\ell^-}$ channel, in paticular.

The division of events into categories based on the number of reconstructed jets allows the analysis discriminants to separate differing contributions of signal and background processes more effectively. The signal production mechanisms considered are $gg \to H \to W^+W^-$, $WH + ZH \to jjW^+W^-$, and vector-boson fusion. The relative fractions of the contributions from each of the three signal processes and background processes, notably $W^+W^-$ production and $t\bar{t}$ production, are very different in the different jet categories. Dividing our data into these categories provides more statistical discrimination, but introduces the need to evaluate the systematic uncertainties carefully in each jet category. A discussion of these uncertainties is found in Section III.

The $H \to W^+W^-$ analyses use neural-network outputs, including likelihoods constructed from calculated matrix-element probabilities as additional inputs for the 0-jet bin.

We include a separate analysis of events with same-sign leptons to incorporate additional potential signal from associated production events in which the two leptons (one from the associated vector boson and one from a $W$ boson produced in the Higgs boson decay) have the same charge. We additionally incorporate three tri-lepton channels to include additional associated production contributions where leptons result from the associated $W$ boson and the two $W$ bosons produced in the Higgs boson decay or where an associated $Z$ boson decays into a dilepton pair and a third lepton is produced in the decay of either of the W bosons resulting from the Higgs decay. In the latter case, the sample is separated into one jet and two or more jet sub-channels to fully take advantage of the Higgs boson mass constraint available in the two or more jet case where all of the decay products are reconstructed.

For the first time we include a search for $H \to ZZ$ using four lepton events. A simple four-lepton invariant mass discriminant is used to separate potential Higgs signal events from the non-resonant $ZZ$ background. Our opposite-sign channels in which one of the two lepton candidates is a hadronic tau are also updated. Events are separated into $e$-$\tau$ and $\mu$-$\tau$ channels. The final discriminants are obtained from boosted decision trees which incorporate both hadronic tau identification and kinematic event variables as inputs.

We include an updated, generic analysis searching for Higgs bosons decaying to tau lepton pairs incorporating contributions from direct $gg \to H$ production, associated $WH$ or $ZH$ production, and vector boson production. We also include for the first time an analysis of events that contain one reconstructed lepton ($\ell = e$ or $\mu$) in addition to a tau lepton pair focusing on associated production where $H \to \tau\tau$ and an additional lepton is produced in the decay of the $W$ or $Z$ boson. For the generic search events with either one or two jets are separated into two independent analysis channels. The final discriminant for setting limits is obtained using four boosted signal tree discriminants, each designed to discriminate the signal against one of the major backgrounds (QCD multi-jets, $W$ plus jets, $Z/\gamma^* \to \tau^+\tau^-$, and $Z/\gamma^* \to \ell^+\ell^-$ where $\ell = e$ or $\mu$). In the new analysis events are separated into three trilpeton categories ($e$-$\mu$-$\tau_{had}$, $\ell$-$\ell$-$\tau_{had}$, and $\ell$-$\tau_{had}$-$\tau_{had}$). The final discriminants are likelihoods based on Support Vector Machine (SVM) outputs obtained using separate trainings for the signal against each of the primary backgrounds ($Z$ plus jets, $t\bar{t}$, and dibosons).

We incorporate an older all-hadronic analysis, which results in two $b$-tagging sub-channels (TDT and LDT) for both $WH/ZH$ and VBF production to the $jjb\bar{b}$ final state. Events with either four or five reconstructed jets are selected, and at least two must be $b$-tagged. The large QCD multi-jet backgrounds are modeled from the data by applying a measured mistag probability to the non $b$-tagged jets in events containing a single $b$-tag. Neural network discriminants based on kinematic event variables including ones designed to separate quark and gluon jets are used to obtain the final limits.

Also included in the combination is an analysis that seeks the decay $H \to \gamma\gamma$. This analysis looks for a signal peak in the diphoton invariant mass spectrum above the smooth background originating from standard QCD production. The signal acceptance has been increased in the updated analysis by including forward (plug) calorimeter candidates

as well as central photon conversion candidates. Events are now separated into four independent analysis channels based on the photon candidates contained within the event: two central candidates (CC), one central and one plug candidate (CP), one central and one central conversion candidate (CC-Conv), or one plug and one central conversion candidate (CP-Conv).

We include for the first time three independent analysis channels searching for the process $t\bar{t}H \rightarrow t\bar{t}b\bar{b}$. One category includes events with a reconstructed lepton, large missing transverse energy, and four or five reconstructed jets. These events are further sub-divided into five $b$-tagging categories (three tight $b$-tags (TTT), two tight and one loose $b$-tags (TTL) , one tight and two loose $b$-tags (TLL), two tight $b$-tags (TDT), and one tight and one loose $b$-tags (LDT)). Ensembles of neural network discriminants trained at each mass point are used to set limits. Events with no reconstructed lepton are separated into two categories, one containing events with large missing transverse energy and five to nine reconstructed jets and another containing events with low missing transverse energy and seven to ten reconstructed jets. Events in these two channels are required to have a minimum of two $b$-tagged jets based on a neural network tagging algorithm. Events with three or more $b$-tags are analyzed in separate channels from those with exactly two tags. Two stages of neural network discriminants are used (the first to help reject large multi-jet backgrounds and the second to separate potential $t\bar{t}H$ signal events from $t\bar{t}$ background events).

Events from QCD multijet (instrumental) backgrounds are typically measured in independent data samples using several different methods. For CDF, backgrounds from SM processes with electroweak gauge bosons or top quarks were generated using PYTHIA, ALPGEN [52], MC@NLO [53], and HERWIG [54] programs. These background processes were normalized using either experimental data or next-to-leading order calculations (including MCFM [56] for the $W+$ heavy flavor process).

## III. SIGNAL PREDICTIONS

We normalize our Higgs boson signal predictions to the most recent high-order calculations available. The $gg \rightarrow H$ production cross section we use is calculated at next-to-next-to leading order (NNLO) in QCD with a next-to-next-to leading log (NNLL) resummation of soft gluons; the calculation also includes two-loop electroweak effects and handling of the running $b$ quark mass [19, 20]. The numerical values in Table I are updates [21] of these predictions with $m_t$ set to 173.1 GeV/$c^2$ [22], and an exact treatment of the massive top and bottom loop corrections up to next-to-leading-order (NLO) + next-to-leading-log factorization and renormalization scale choice for this calculation is $\mu_F = \mu_R = m_H$. These calculations are refinements of the earlier NNLO calculations of the $gg \rightarrow H$ production cross section [25–27]. Electroweak corrections were computed in Refs. [28, 29]. Soft gluon resummation was introduced in the prediction of the $gg \rightarrow H$ production cross section in Ref. [30]. The $gg \rightarrow H$ production cross section depends strongly on the gluon parton density function, and the accompanying value of $\alpha_s(q^2)$. The cross sections used here are calculated with the MSTW 2008 NNLO PDF set [31], as recommended by the PDF4LHC working group [32]. The inclusive Higgs boson production cross sections are listed in Table I.

For analyses that consider inclusive $gg \rightarrow H$ production but do not split it into separate channels based on the number of reconstructed jets, we use the inclusive uncertainties from the simultaneous variation of the factorization and renormalization scale up and down by a factor of two. We use the prescription of the PDF4LHC working group for evaluating PDF uncertainties on the inclusive production cross section. QCD scale uncertainties that affect the cross section via their impacts on the PDFs are included as a correlated part of the total scale uncertainty. The remainder of the PDF uncertainty is treated as uncorrelated with the QCD scale uncertainty.

For analyses seeking $gg \rightarrow H$ production that divide events into categories based on the number of reconstructed jets, we employ a new approach for evaluating the impacts of the scale uncertainties. Following the recommendations of Ref. [23], we treat the QCD scale uncertainties obtained from the NNLL inclusive [19, 20], NLO one or more jets [18], and NLO two or more jets [24] cross section calculations as uncorrelated with one another. We then obtain QCD scale uncertainties for the exclusive $gg \rightarrow H + 0$ jet, 1 jet, and 2 or more jet categories by propagating the uncertainties on the inclusive cross section predictions through the subtractions needed to predict the exclusive rates. For example, the $H$+0 jet cross section is obtained by subtracting the NLO $H + 1$ or more jet cross section from the inclusive NNLL+NNLO cross section. We now assign three separate, uncorrelated scale uncertainties which lead to correlated and anticorrelated uncertainty contributions between exclusive jet categories. The procedure in Ref. [18] is used to determine PDF model uncertainties. These are obtained separately for each jet bin.

We include all significant Higgs production modes in the high-mass search. Besides gluon-gluon fusion through virtual quark loops (ggH), we include Higgs boson production in association with a $W$ or $Z$ vector boson (VH), and vector boson fusion (VBF). For the low-mass searches, we target the $WH$, $ZH$, VBF, and $t\bar{t}H$ [39] production modes with specific searches, including also those signal components not specifically targeted but which fall in the acceptance nonetheless. Our $WH$ and $ZH$ cross sections are from Ref. [40]. This calculation starts with the NLO calculation of V2HV [41] and includes NNLO QCD contributions [42], as well as one-loop electroweak corrections [43]. We use the VBF cross section computed at NNLO in QCD in Ref. [44]. Electroweak corrections to the VBF production cross section are computed with the HAWK program [45], and are small and negative (2-3%) in the Higgs boson mass range considered here. We include these corrections in the VBF cross sections used for this result. The $t\bar{t}H$ production cross sections we use are from Ref. [39].

In order to predict the kinematic distributions of Higgs boson signal events, we use the PYTHIA [46] Monte Carlo program, with CTEQ5L and CTEQ6L [47] leading-order (LO) parton distribution functions. The Higgs boson decay branching ratio predictions used for this result are those of Ref. [48]. In this calculation, the partial decay widths for all Higgs boson decays except to pairs of $W$ and $Z$ bosons are computed with HDECAY [49], and the $W$ and $Z$ pair decay widths are computed with PROPHECY4F [50]. The relevant decay branching ratios are listed in Table I. The uncertainties on the predicted branching ratios from uncertainties in $m_b$, $m_c$, and $\alpha_s$ are presented in Ref. [51].

Table II summarizes the integrated luminosities, the Higgs boson mass ranges over which the searches are performed, and references to further details for each analysis.

## IV. DISTRIBUTIONS OF CANDIDATES

All analyses provide binned histograms of the final discriminant variables for the signal and background predictions, itemized separately for each source, and the observed data. The number of channels combined is large, and the number of bins in each channel is large. Therefore, the task of assembling histograms and checking whether the expected and observed limits are consistent with the input predictions and observed data is difficult. We therefore provide histograms that aggregate all channels' signal, background, and data together. In order to preserve most of the sensitivity gain that is achieved by the analyses by binning the data instead of collecting them all together and counting, we aggregate the data and predictions in narrow bins of signal-to-background ratio, $s/b$. Data with similar $s/b$ may be added together with no loss in sensitivity, assuming similar systematic errors on the predictions. The aggregate histograms do not show the effects of systematic uncertainties, but instead compare the data with the central predictions supplied by each analysis.

The range of $s/b$ is quite large in each analysis, and so $\log_{10}(s/b)$ is chosen as the plotting variable. Plots of the distributions of $\log_{10}(s/b)$ are shown for Higgs boson masses of 115 and 165 GeV/$c^2$ in Figure 1. These distributions can be integrated from the high-$s/b$ side downwards, showing the sums of signal, background, and data for the most pure portions of the selection of all channels added together. These integrals can be seen in Figure 2. The most significant candidates are found in the bins with the highest $s/b$; an excess in these bins relative to the background prediction drives the Higgs boson cross section limit upwards, while a deficit drives it downwards. The lower-$s/b$ bins show that the modeling of the rates and kinematic distributions of the backgrounds is very good. The integrated plots show a slight excess of events in the highest-$s/b$ bins for the analyses seeking a Higgs boson mass of 115 GeV/$c^2$, and a slight deficit of events in the highest-$s/b$ bins for the analyses seeking a Higgs boson of mass 165 GeV/$c^2$.

We also show the distributions of the data after subtracting the expected background, and compare that with the expected signal yield for a Standard Model Higgs boson, after collecting all bins in all channels sorted by $s/b$. These background-subtracted distributions are shown in Figure 3. These graphs also show the remaining uncertainty on the background prediction after fitting the background model to the data within the systematic uncertainties on the rates and shapes in each contributing channel's templates.

TABLE I: The production cross sections and decay branching fractions for the SM Higgs boson assumed for the combination.

| $m_H$ ($\mathrm{GeV}/c^2$) | $\sigma_{gg\to H}$ (fb) | $\sigma_{WH}$ (fb) | $\sigma_{ZH}$ (fb) | $\sigma_{VBF}$ (fb) | $\sigma_{t\bar{t}H}$ (fb) | $B(H\to b\bar{b})$ (%) | $B(H\to c\bar{c})$ (%) | $B(H\to\tau^+\tau^-)$ (%) | $B(H\to W^+W^-)$ (%) | $B(H\to ZZ)$ (%) | $B(H\to\gamma\gamma)$ (%) |
|---|---|---|---|---|---|---|---|---|---|---|---|
| 100 | 1821.8 | 291.90 | 169.8 | 97.2 | 8.000 | 79.1 | 3.68 | 8.36 | 1.11 | 0.113 | 0.159 |
| 105 | 1584.7 | 248.40 | 145.9 | 89.7 | 7.062 | 77.3 | 3.59 | 8.25 | 2.43 | 0.215 | 0.178 |
| 110 | 1385.0 | 212.00 | 125.7 | 82.7 | 6.233 | 74.5 | 3.46 | 8.03 | 4.82 | 0.439 | 0.197 |
| 115 | 1215.9 | 174.50 | 103.9 | 76.4 | 5.502 | 70.5 | 3.27 | 7.65 | 8.67 | 0.873 | 0.213 |
| 120 | 1072.3 | 150.10 | 90.2 | 70.7 | 4.857 | 64.9 | 3.01 | 7.11 | 14.3 | 1.60 | 0.225 |
| 125 | 949.3 | 129.50 | 78.5 | 65.3 | 4.279 | 57.8 | 2.68 | 6.37 | 21.6 | 2.67 | 0.230 |
| 130 | 842.9 | 112.00 | 68.5 | 60.4 | 3.769 | 49.4 | 2.29 | 5.49 | 30.5 | 4.02 | 0.226 |
| 135 | 750.8 | 97.20 | 60.0 | 55.9 | 3.320 | 40.4 | 1.87 | 4.52 | 40.3 | 5.51 | 0.214 |
| 140 | 670.6 | 84.60 | 52.7 | 51.8 | 2.925 | 31.4 | 1.46 | 3.54 | 50.4 | 6.92 | 0.194 |
| 145 | 600.6 | 73.70 | 46.3 | 48.1 | 2.593 | 23.1 | 1.07 | 2.62 | 60.3 | 7.96 | 0.168 |
| 150 | 539.1 | 64.40 | 40.8 | 44.6 | 2.298 | 15.7 | 0.725 | 1.79 | 69.9 | 8.28 | 0.137 |
| 155 | 484.0 | 56.20 | 35.9 | 41.2 | 2.037 | 9.18 | 0.425 | 1.06 | 79.6 | 7.36 | 0.100 |
| 160 | 432.3 | 48.50 | 31.4 | 38.2 | 1.806 | 3.44 | 0.159 | 0.397 | 90.9 | 4.16 | 0.0533 |
| 165 | 383.7 | 43.60 | 28.4 | 36.0 | 1.607 | 1.19 | 0.0549 | 0.138 | 96.0 | 2.22 | 0.0230 |
| 170 | 344.0 | 38.50 | 25.3 | 33.4 | 1.430 | 0.787 | 0.0364 | 0.0920 | 96.5 | 2.36 | 0.0158 |
| 175 | 309.7 | 34.00 | 22.5 | 31.0 | 1.272 | 0.612 | 0.0283 | 0.0719 | 95.8 | 3.23 | 0.0123 |
| 180 | 279.2 | 30.10 | 20.0 | 28.8 | 1.132 | 0.497 | 0.0230 | 0.0587 | 93.2 | 6.02 | 0.0102 |
| 185 | 252.1 | 26.90 | 17.9 | 26.9 | 1.004 | 0.385 | 0.0178 | 0.0457 | 84.4 | 15.0 | 0.00809 |
| 190 | 228.0 | 24.00 | 16.1 | 25.0 | 0.890 | 0.315 | 0.0146 | 0.0376 | 78.6 | 20.9 | 0.00674 |
| 195 | 207.2 | 21.40 | 14.4 | 23.3 | 0.789 | 0.270 | 0.0125 | 0.0324 | 75.7 | 23.9 | 0.00589 |
| 200 | 189.1 | 19.10 | 13.0 | 21.6 | 0.700 | 0.238 | 0.0110 | 0.0287 | 74.1 | 25.6 | 0.00526 |

TABLE II: Luminosity, explored mass range and references for the different processes and final states ($\ell = e$ or $\mu$) for the CDF analyses. The generic labels "2×" and "4×" refer to separations based on lepton categories.

| Channel | Luminosity ($\text{fb}^{-1}$) | $m_H$ range ($\text{GeV}/c^2$) | Reference |
|---|---|---|---|
| $WH \to \ell\nu b\bar{b}$ 2-jet channels 4×(TDT,LDT,ST,LDTX) | 7.5 | 100-150 | [5] |
| $WH \to \ell\nu b\bar{b}$ 3-jet channels 2×(TDT,LDT,ST) | 5.6 | 100-150 | [6] |
| $ZH \to \nu\bar{\nu}b\bar{b}$ (TDT,LDT,ST) | 7.8 | 100-150 | [7] |
| $ZH \to \ell^+\ell^- b\bar{b}$ 2×(TDT,LDT,ST) | 7.7 | 100-150 | [8, 9] |
| $H \to W^+W^-$ 2×(0 jets,1 jet)+(2 or more jets)+(low-$m_{\ell\ell}$)+($e$-$\tau_{had}$)+($\mu$-$\tau_{had}$) | 8.2 | 110-200 | [10] |
| $WH \to WW^+W^-$ (same-sign leptons)+(tri-leptons) | 8.2 | 110-200 | [10] |
| $ZH \to ZW^+W^-$ (tri-leptons with 1 jet)+(tri-leptons with 2 or more jets) | 8.2 | 110-200 | [10] |
| $H \to Z^\circ Z^\circ \to \ell^+\ell^-\ell^+\ell^-$ | 8.2 | 110-200 | [11] |
| $H + X \to \tau^+\tau^-$ (1 jet)+(2 jets) | 6.0 | 100-150 | [12] |
| $WH \to \ell\nu\tau^+\tau^-/ZH \to \ell^+\ell^-\tau^+\tau^-$ ($\ell$-$\ell$-$\tau_{had}$)+($e$-$\mu$-$\tau_{had}$)+($\ell$-$\tau_{had}$-$\tau_{had}$) | 6.2 | 110-150 | [13] |
| $WH + ZH \to jjb\bar{b}$ (GF,VBF)×(TDT,LDT) | 4.0 | 100-150 | [14] |
| $H \to \gamma\gamma$ (CC,CP,CC-Conv,CP-Conv) | 7.0 | 100-150 | [15] |
| $t\bar{t}H \to WWb\bar{b}b\bar{b}$ (lepton) (4jet,5jet)×(TTT,TTL,TLL,TDT,LDT) | 6.3 | 100-150 | [16] |
| $t\bar{t}H \to WWb\bar{b}b\bar{b}$ (no lepton) (low met,high met)×(2 tags,3 or more tags) | 5.7 | 100-150 | [17] |

## V. COMBINING CHANNELS

We combine the results of the searches using a Bayesian technique, which is described below. Both methods rely on distributions in the final discriminants, and not just on their single integrated values. Systematic uncertainties enter on the predicted number of signal and background events as well as on the distribution of the discriminants in each analysis ("shape uncertainties"). Both methods use likelihood calculations based on Poisson probabilities.

### A. Statistical Method

We choose to use a Bayesian statistical method [3], with a flat prior assumed for the total number of selected Higgs events. For a given Higgs boson mass, the combined likelihood is a product of likelihoods for the individual channels, each of which is a product over histogram bins:

$$\mathcal{L}(R, \vec{s}, \vec{b}|\vec{n}, \vec{\theta}) \times \pi(\vec{\theta}) = \prod_{i=1}^{N_C} \prod_{j=1}^{N_b} \mu_{ij}^{n_{ij}} e^{-\mu_{ij}} / n_{ij}! \times \prod_{k=1}^{n_{np}} e^{-\theta_k^2/2} \quad (1)$$

where the first product is over the number of channels ($N_C$), and the second product is over $N_b$ histogram bins containing $n_{ij}$ events, binned in ranges of the final discriminants used for individual analyses, such as the dijet mass, neural-network outputs, or matrix-element likelihoods. The parameters that contribute to the expected bin contents are $\mu_{ij} = R \times s_{ij}(\vec{\theta}) + b_{ij}(\vec{\theta})$ for the channel $i$ and the histogram bin $j$, where $s_{ij}$ and $b_{ij}$ represent the expected background and signal in the bin, and $R$ is a scaling factor applied to the signal to test the sensitivity level of the experiment. Truncated Gaussian priors are used for each of the nuisance parameters $\theta_k$, which define the sensitivity of the predicted signal and background estimates to systematic uncertainties. These can take the form of uncertainties on overall rates, as well as the shapes of the distributions used for combination. These systematic uncertainties can be far larger than the expected SM Higgs boson signal, and are therefore important in the calculation of limits. The truncation is applied so that no prediction of any signal or background in any bin is negative. The posterior density function is then integrated over all parameters (including correlations) except for $R$, and a 95% credibility level upper limit on $R$ is estimated by calculating the value of $R$ that corresponds to 95% of the area of the resulting distribution.

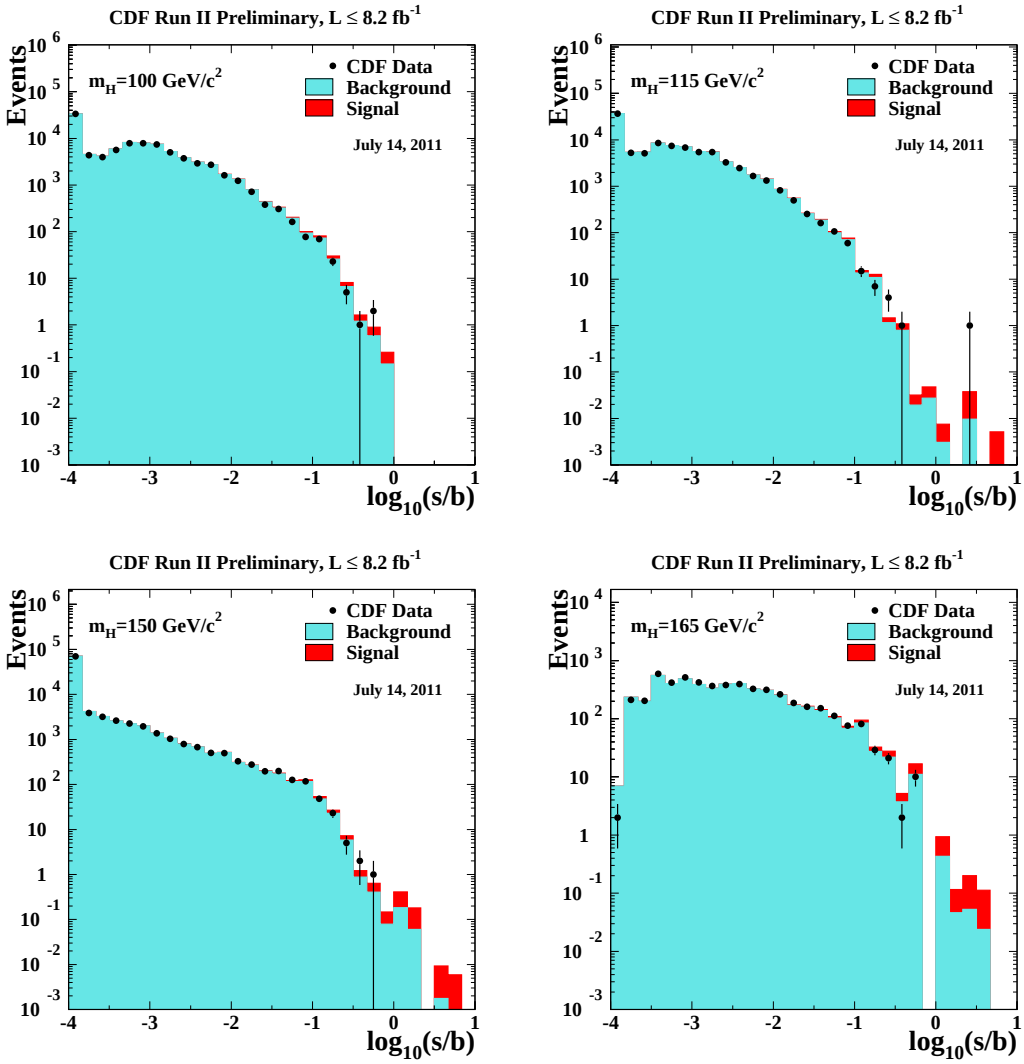


FIG. 1: Distributions of $\log_{10}(s/b)$, for the data from all contributing channels, for Higgs boson masses of 100, 115, 150, 165, and 200 GeV/$c^2$. The data are shown with points, and the expected signal is shown stacked on top of the backgrounds. Underflows and overflows are collected into the bottom and top bins.

### B. Systematic Uncertainties

Systematic uncertainties differ between analyses, and they affect the rates and shapes of the predicted signal and background in correlated ways. The combined results incorporate the sensitivity of predictions to values of nuisance parameters, and include correlations between rates and shapes, between signals and backgrounds, and between channels. More on these issues can be found in the individual analysis notes [5] through [17]. Here we consider only the largest contributions and correlations between and within the two experiments.

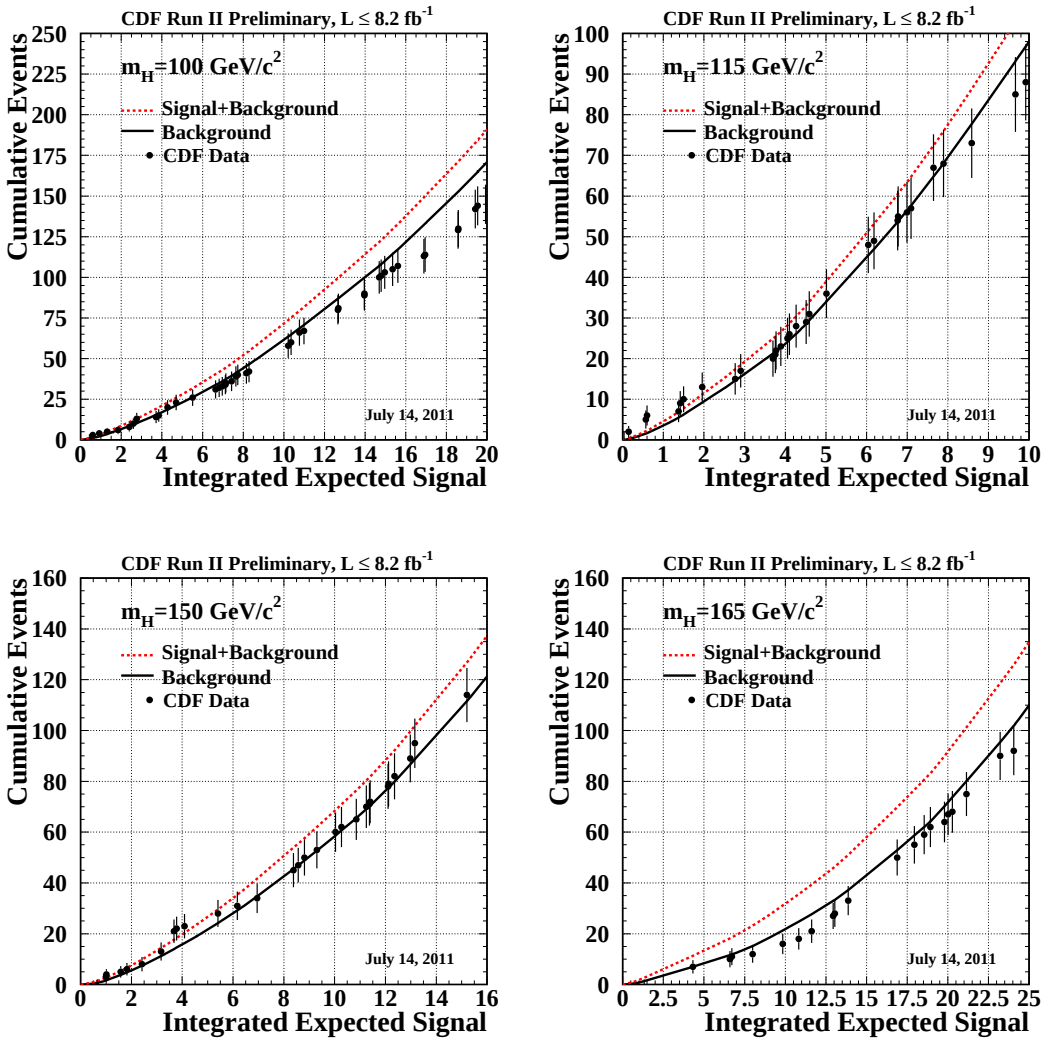


FIG. 2: Integrated distributions of $s/b$, starting at the high $s/b$ side, for Higgs boson masses of 100, 115, 150, and 165 GeV/$c^2$. The total signal+background and background-only integrals are shown separately, along with the data sums. Data are only shown for bins that have data events in them.

### *1. Correlated Systematics Between Channels*

The uncertainty on the measurement of the integrated luminosity is 6%. Of this value, 4% arises from the uncertainty on the inelastic $p\bar{p}$ scattering cross section. All predictions of signals and backgrounds that rely on theoretical cross section predictions that are scaled by the integrated luminosity share this common source of systematic uncertainty. Most channels presented here also share the assumed values and uncertainties on the production cross sections for top-quark processes ($t\bar{t}$ and single top) and for electroweak processes ($WW$, $WZ$, and $ZZ$). In order to provide a consistent combination, the values of these cross sections assumed in each analysis are brought into agreement. We use $\sigma_{t\bar{t}} = 7.04^{+0.24}_{-0.36}$ (scale) $\pm$ 0.14(PDF) $\pm$ 0.30(mass), following the calculation of Moch and Uwer [59], assuming a top quark mass $m_t = 173.0 \pm 1.2$ GeV/$c^2$ [60], and using the MSTW2008nnlo PDF set [31]. Other calculations of $\sigma_{t\bar{t}}$

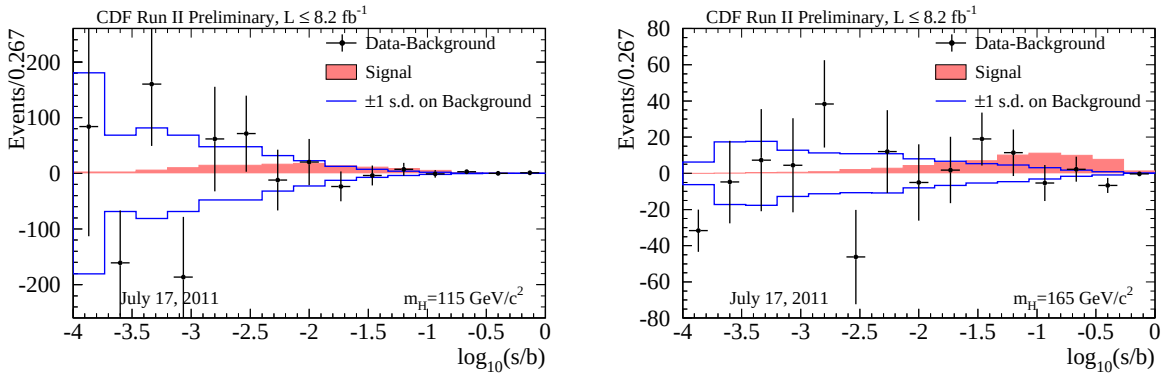


FIG. 3: Background-subtracted data distributions for all channels, summed in bins of $s/b$, for Higgs boson masses of 115 and 165 GeV/$c^2$. The background has been fit, within its systematic uncertainties, to the data. The points with error bars indicate the background-subtracted data; the sizes of the error bars are the square roots of the predicted background in each bin. The unshaded (blue-outline) histogram shows the systematic uncertainty on the best-fit background model, and the shaded histogram shows the expected signal for a Standard Model Higgs boson.

are similar [61].

For single top, we use the NLL $t$-channel calculation of Kidonakis [62], which has been updated using the MSTW2008nnlo PDF set [31] [63]. For the $s$-channel process we use [64], again based on the MSTW2008nnlo PDF set. Both of the cross section values below are the sum of the single $t$ and single $\bar{t}$ cross sections, and both assume $m_t = 173 \pm 1.2$ GeV.

$$\sigma_{t-\mathrm{chan}} = 2.10 \pm 0.027(\mathrm{scale}) \pm 0.18(\mathrm{PDF}) \pm 0.045(\mathrm{mass})\mathrm{pb}. \quad (2)$$

$$\sigma_{s-\mathrm{chan}} = 1.046 \pm 0.006(\mathrm{scale}) \pm 0.059\ (\mathrm{PDF}) \pm 0.030\ (\mathrm{mass})\ \mathrm{pb}. \quad (3)$$

Other calculations of $\sigma_{\mathrm{SingleTop}}$ are similar for our purposes [65].

MCFM [56] has been used to compute the NLO cross sections for $WW$, $WZ$, and $ZZ$ production [66]. Using a scale choice $\mu_0 = M_V^2 + p_T^2(V)$ and the MSTW2008 PDF set [31], the cross section for inclusive $W^+W^-$ production is

$$\sigma_{W^+W^-} = 11.34^{+0.56}_{-0.49}\ (\mathrm{scale})\ ^{+0.35}_{-0.28}(\mathrm{PDF})\mathrm{pb} \quad (4)$$

and the cross section for inclusive $W^{\pm}Z$ production is

$$\sigma_{W^{\pm}Z} = 3.22^{+0.20}_{-0.17}\ (\mathrm{scale})\ ^{+0.11}_{-0.08}\ (\mathrm{PDF})\ \mathrm{pb} \quad (5)$$

For the $Z$, leptonic decays are used in the definition, with both $\gamma$ and $Z$ exchange. The cross section quoted above involves the requirement $75 \leq m_{\ell^+\ell^-} \leq 105$ GeV for the leptons from the neutral current exchange. The same dilepton invariant mass requirement is applied to both sets of leptons in determining the $ZZ$ cross section which is

$$\sigma_{ZZ} = 1.20^{+0.05}_{-0.04}\ (\mathrm{scale})\ ^{+0.04}_{-0.03}\ (\mathrm{PDF})\ \mathrm{pb} \quad (6)$$

For the diboson cross section calculations, $|\eta_\ell| < 5$ for all calculations. Loosening this requirement to include all leptons leads to $\sim$+0.4% change in the predictions. Lowering the factorization and renormalization scales by a factor of two increases the cross section, and raising the scales by a factor of two decreases the cross section. The PDF uncertainty has the same fractional impact on the predicted cross section independent of the scale choice. All PDF

uncertainties are computed as the quadrature sum of the twenty 68% C.L. eigenvectors provided with MSTW2008 (MSTW2008nlo68cl).

In many analyses, the dominant background yields are calibrated with data control samples. Since the methods of measuring the multijet ("QCD") backgrounds differ between analyses, there is no correlation assumed between these rates. Similarly, the large uncertainties on the background rates for $W$+heavy flavor (HF) and $Z$+heavy flavor are considered at this time to be uncorrelated, as the several analyses which are sensitive to this parameter employ different techniques to estimate its central value, which is obscured by effects of acceptance and efficiency being different between the analyses. The calibrations of fake leptons, unvetoed $\gamma \to e^+e^-$ conversions, $b$-tag efficiencies and mistag rates are performed by each collaboration using independent data samples and methods, and are therefore also treated as uncorrelated.

### *2. Systematic Uncertainties for Each Channel*

The dominant systematic uncertainties for the analyses combined in this note are shown in the Appendix in Tables IV and V for the $WH \to \ell\nu b\bar{b}$ channels, in Table VI for the $WH, ZH \to \not\!\!E_T b\bar{b}$ channels, in Tables VII and VIII for the $ZH \to \ell^+\ell^- b\bar{b}$ channels, in Tables IX, X, and XI for the $H \to W^+W^- \to \ell'^{\pm}\nu\ell'^{\mp}\nu$ channels, in Table XII for the $WH \to WWW \to \ell'^{\pm}\ell'^{\pm}$ and $WH \to WWW \to \ell^{\pm}\ell'^{\pm}\ell''^{\mp}$ channels, in Table XIII for the $ZH \to ZWW \to \ell^{\pm}\ell^{\mp}\ell'^{\pm}$ channels, In Table XIV for the $H \to 4\ell$ channel, in Tables XV, XVI, and XVII for the $t\bar{t}H \to W^+bW^-\bar{b}b\bar{b}$ channels, in Table XVIII for the $H \to \tau^+\tau^-$ channels, in Table XIX for the $WH \to \ell\nu\tau^+\tau^-$ and $ZH \to \ell^+\ell^-\tau^+\tau^-$ channels, in Table XX for the $WH/ZH$ and VBF $\to jjb\bar{b}$ channels, and in Table XXI for the $H \to \gamma\gamma$ channel. Each source induces a correlated uncertainty across all CDF channels' signal and background contributions which are sensitive to that source. For $H \to b\bar{b}$, the largest uncertainties on signal arise from measured $b$-tagging efficiencies, jet energy scale, and other Monte Carlo modeling. Shape dependencies of templates on jet energy scale, $b$-tagging, and gluon radiation ("ISR" and "FSR") are taken into account for some analyses (see tables). For $H \to W^+W^-$, the largest uncertainties on signal acceptance originate from Monte Carlo modeling. Uncertainties on background event rates vary significantly for the different processes. The backgrounds with the largest systematic uncertainties are in general quite small. Such uncertainties are constrained by fits to the nuisance parameters, and they do not affect the result significantly. Because the largest background contributions are measured using data, these uncertainties are treated as uncorrelated for the $H \to b\bar{b}$ channels. The differences in the resulting limits when treating the remaining uncertainties as either correlated or uncorrelated, is less than 5%.

## VI. COMBINED RESULTS

Using the combination procedure outlined in Section III, we extract limits on SM Higgs boson production $\sigma \times B(H \to X)$ in $p\bar{p}$ collisions at $\sqrt{s} = 1.96$ TeV for $100 \leq m_H \leq 200$ GeV/$c^2$. To facilitate comparisons with the standard model and to accommodate analyses with different degrees of sensitivity, we present our results in terms of the ratio of obtained limits to the SM Higgs boson production cross section, as a function of Higgs boson mass, for test masses for which we have performed dedicated searches in different channels. A value of the combined limit ratio which is less than or equal to one indicates that that particular Higgs boson mass is excluded at the 95% C.L.

The combinations of CDF's search results yield the following ratios of 95% C.L. observed (expected) limits to the SM cross section: 1.55 (1.49) $m_H = 115$ GeV/$c^2$, and 0.75 (0.79) at $m_H = 165$ GeV/$c^2$.

The ratios of the 95% C.L. expected and observed limit to the SM cross section are shown in Figure 4 for the combined CDF analyses. The observed and median expected ratios are listed for the tested Higgs boson masses in Table III.

In summary, we combine all available CDF results on SM Higgs boson searches, based on luminosities ranging from 4.0 to 8.2 fb$^{-1}$. Compared to our previous combination, more data have been added to the existing channels, additional channels have been included, and analyses have been further optimized to gain sensitivity. We use the

latest parton distribution functions and $gg \rightarrow H$ theoretical cross sections when comparing our limits to the SM predictions at high mass.

The 95% C.L. upper limits on Higgs boson production are a factor of 1.17 and 0.48 times the SM cross section for a Higgs boson mass of $m_H$ =115 and 165 GeV/$c^2$, respectively. Based on simulation, the corresponding median expected upper limits are 1.16 and 0.57, respectively. Standard Model branching ratios, calculated as functions of the Higgs boson mass, are assumed.

We choose to use the intersections of piecewise linear interpolations of our observed and expected rate limits in order to quote ranges of Higgs boson masses that are excluded and that are expected to be excluded. The sensitivities of our searches to Higgs bosons are smooth functions of the Higgs boson mass and depend most strongly on the predicted cross sections and the decay branching ratios (the decay $H \rightarrow W^+W^-$ is the dominant decay for the region of highest sensitivity). The mass resolution of the channels is poor due to the presence of two highly energetic neutrinos in signal events. We therefore use the linear interpolations to extend the results from the 5 GeV/$c^2$ mass grid investigated to points in between. This procedure yields higher expected and observed interpolated limits than

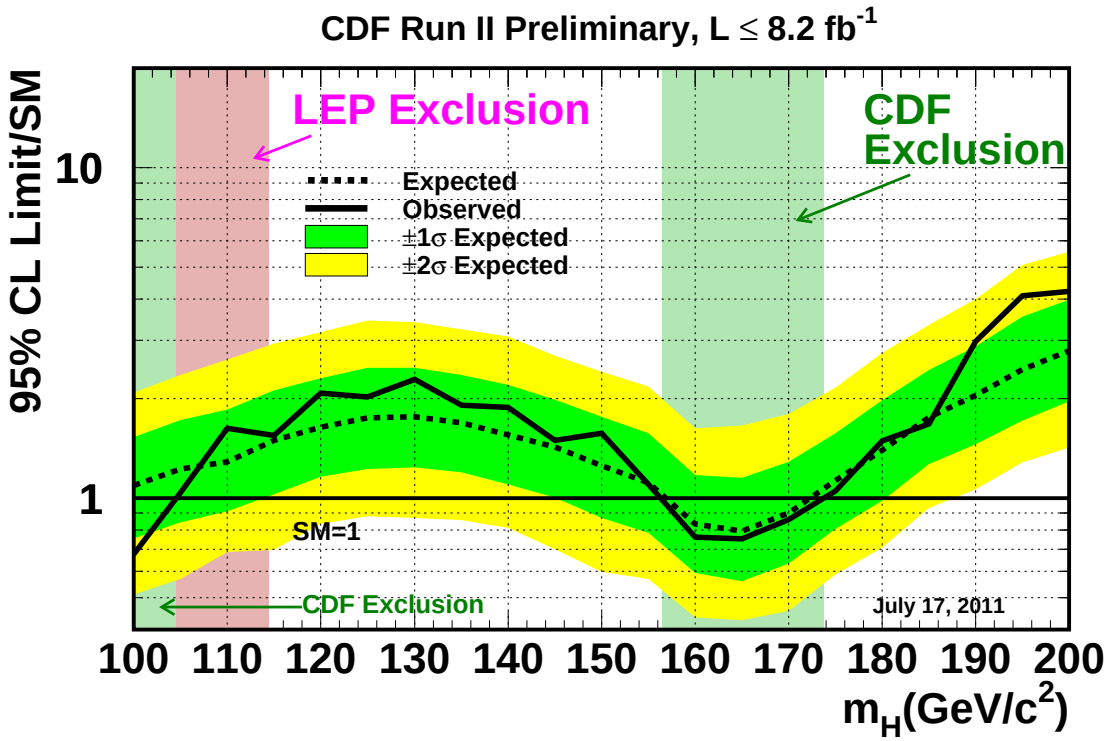


FIG. 4: Observed and expected (median, for the background-only hypothesis) 95% C.L. upper limits on the ratios to the SM cross section, as functions of the Higgs boson mass for the combined CDF and D0 analyses. The limits are expressed as a multiple of the SM prediction for test masses (every 5 GeV/$c^2$) for which both experiments have performed dedicated searches in different channels. The points are joined by straight lines for better readability. The bands indicate the 68% and 95% probability regions where the limits can fluctuate, in the absence of signal.

TABLE III: CDF Run II Preliminary SM Higgs Combination, $L \leq 8.2$ fb$^{-1}$. Limits are listed at the 95% C.L.

| $m_H$ (GeV/$c^2$) | obs (Limit/SM) | $-2\sigma$ exp (Limit/SM) | $-1\sigma$ exp (Limit/SM) | Median exp (Limit/SM) | $+1\sigma$exp (Limit/SM) | $+2\sigma$exp (Limit/SM) |
|---|---|---|---|---|---|---|
| 100 | 0.68 | 0.51 | 0.76 | 1.09 | 1.53 | 2.08 |
| 105 | 1.04 | 0.57 | 0.84 | 1.22 | 1.72 | 2.36 |
| 110 | 1.62 | 0.69 | 0.91 | 1.29 | 1.85 | 2.63 |
| 115 | 1.55 | 0.70 | 1.03 | 1.49 | 2.12 | 2.93 |
| 120 | 2.08 | 0.83 | 1.16 | 1.64 | 2.30 | 3.18 |
| 125 | 2.02 | 0.88 | 1.23 | 1.75 | 2.48 | 3.45 |
| 130 | 2.29 | 0.87 | 1.24 | 1.77 | 2.48 | 3.40 |
| 135 | 1.91 | 0.86 | 1.20 | 1.69 | 2.36 | 3.24 |
| 140 | 1.88 | 0.81 | 1.10 | 1.55 | 2.20 | 3.08 |
| 145 | 1.49 | 0.70 | 1.00 | 1.42 | 1.98 | 2.70 |
| 150 | 1.57 | 0.60 | 0.87 | 1.25 | 1.76 | 2.42 |
| 155 | 1.10 | 0.57 | 0.79 | 1.11 | 1.57 | 2.17 |
| 160 | 0.76 | 0.44 | 0.59 | 0.84 | 1.17 | 1.62 |
| 165 | 0.75 | 0.43 | 0.56 | 0.79 | 1.15 | 1.66 |
| 170 | 0.86 | 0.46 | 0.63 | 0.90 | 1.28 | 1.80 |
| 175 | 1.05 | 0.59 | 0.81 | 1.13 | 1.57 | 2.16 |
| 180 | 1.49 | 0.71 | 0.98 | 1.39 | 1.97 | 2.75 |
| 185 | 1.68 | 0.93 | 1.27 | 1.76 | 2.44 | 3.34 |
| 190 | 2.98 | 1.06 | 1.45 | 2.05 | 2.88 | 3.99 |
| 195 | 4.09 | 1.28 | 1.72 | 2.45 | 3.54 | 5.07 |
| 200 | 4.23 | 1.42 | 1.96 | 2.80 | 3.98 | 5.57 |

if the full dependence of the cross section and branching ratio were included as well, since the latter produces limit curves that are concave upwards. The regions of Higgs boson masses excluded at the 95% C.L. thus obtained are $156.5 < m_H < 173.7$ GeV/$c^2$ and $100 < m_H < 104.5$ GeV/$c^2$. The expected exclusion region, given the current sensitivity, is $157.0 < m_H < 172.2$ GeV/$c^2$.

The results presented in this paper significantly extend the individual limits of each contributing anlaysis and those obtained in our previous combination. The sensitivity of our combined search is sufficient to exclude a Higgs boson at high mass and is expected to grow in the future as more data are added and further improvements are made to our analysis techniques. In Fig. 5 the ratios of the 95% C.L. expected and observed limit to the SM cross section are shown for the combination of the subset of CDF and D0 analyses focusing on the $H \to b\bar{b}$ decay channel. These are the search modes for which we expect Tevatron sensitivity to remain competitive with the LHC experiments for several years moving forward.

**Acknowledgments**

We thank the Fermilab staff and the technical staffs of the participating institutions for their vital contributions. This work was supported by the U.S. Department of Energy and National Science Foundation; the Italian Istituto Nazionale di Fisica Nucleare; the Ministry of Education, Culture, Sports, Science and Technology of Japan; the Natural Sciences and Engineering Research Council of Canada; the National Science Council of the Republic of China; the Swiss National Science Foundation; the A.P. Sloan Foundation; the Bundesministerium für Bildung und Forschung, Germany; the Korean World Class University Program, the National Research Foundation of Korea; the Science and Technology Facilities Council and the Royal Society, UK; the Institut National de Physique Nucleaire et Physique des Particules/CNRS; the Russian Foundation for Basic Research; the Ministerio de Ciencia e Innovación, and Programa Consolider-Ingenio 2010, Spain; the Slovak R&D Agency; the Academy of Finland; and the Australian Research Council (ARC).

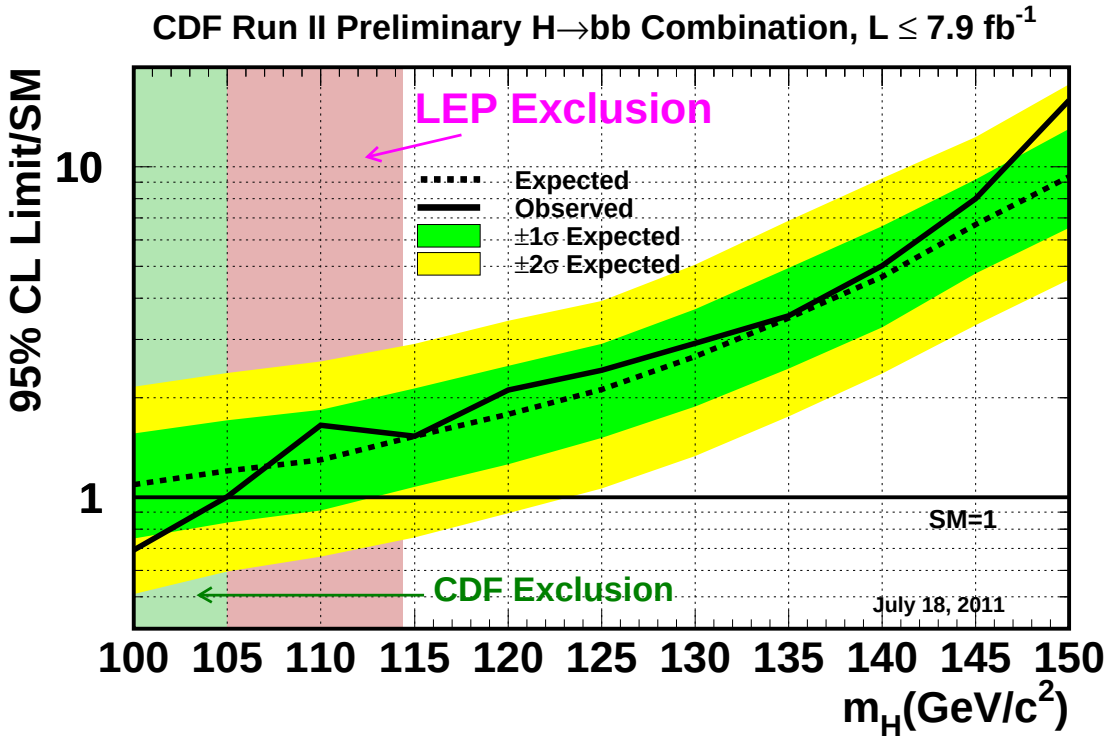


FIG. 5: Observed and expected (median, for the background-only hypothesis) 95% C.L. upper limits on the ratios to the SM cross section, as functions of the Higgs boson mass for the combination of CDF analyses focusing on the $H \to b\bar{b}$ decay channel. The limits are expressed as a multiple of the SM prediction for test masses (every 5 GeV/$c^2$) for which both experiments have performed dedicated searches in different channels. The points are joined by straight lines for better readability. The bands indicate the 68% and 95% probability regions where the limits can fluctuate, in the absence of signal. The limits displayed in this figure are obtained with the Bayesian calculation.

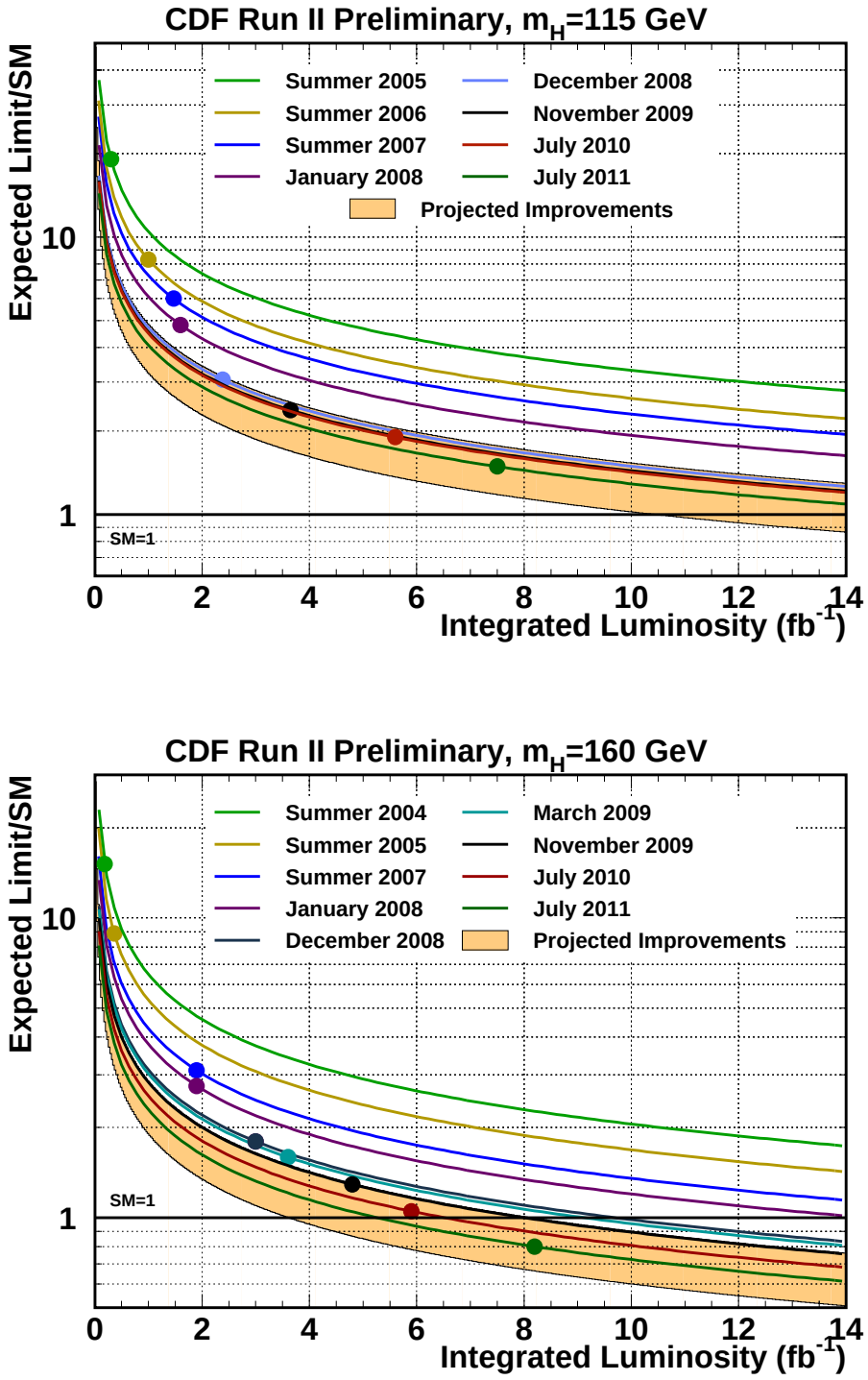


FIG. 6: Sensitivity projections and achieved sensitivities for the combined CDF Higgs boson searches, at $m_H = 115$ and 160 GeV/$c^2$. The curves are proportional to $1/\sqrt{\int Ldt}$ extrapolations of the median expected limits, and each analysis update corresponds to a new point with a new curve. The light orange bands indicate ranges of possible improvements in performance, relative to the Summer 2007 sensitivity. The top of the light orange bands is a factor of 1.5 below the Summer 2007 curve, and the bottom of the light orange bands are a further factor of 1.5 below the top of the light orange bands.

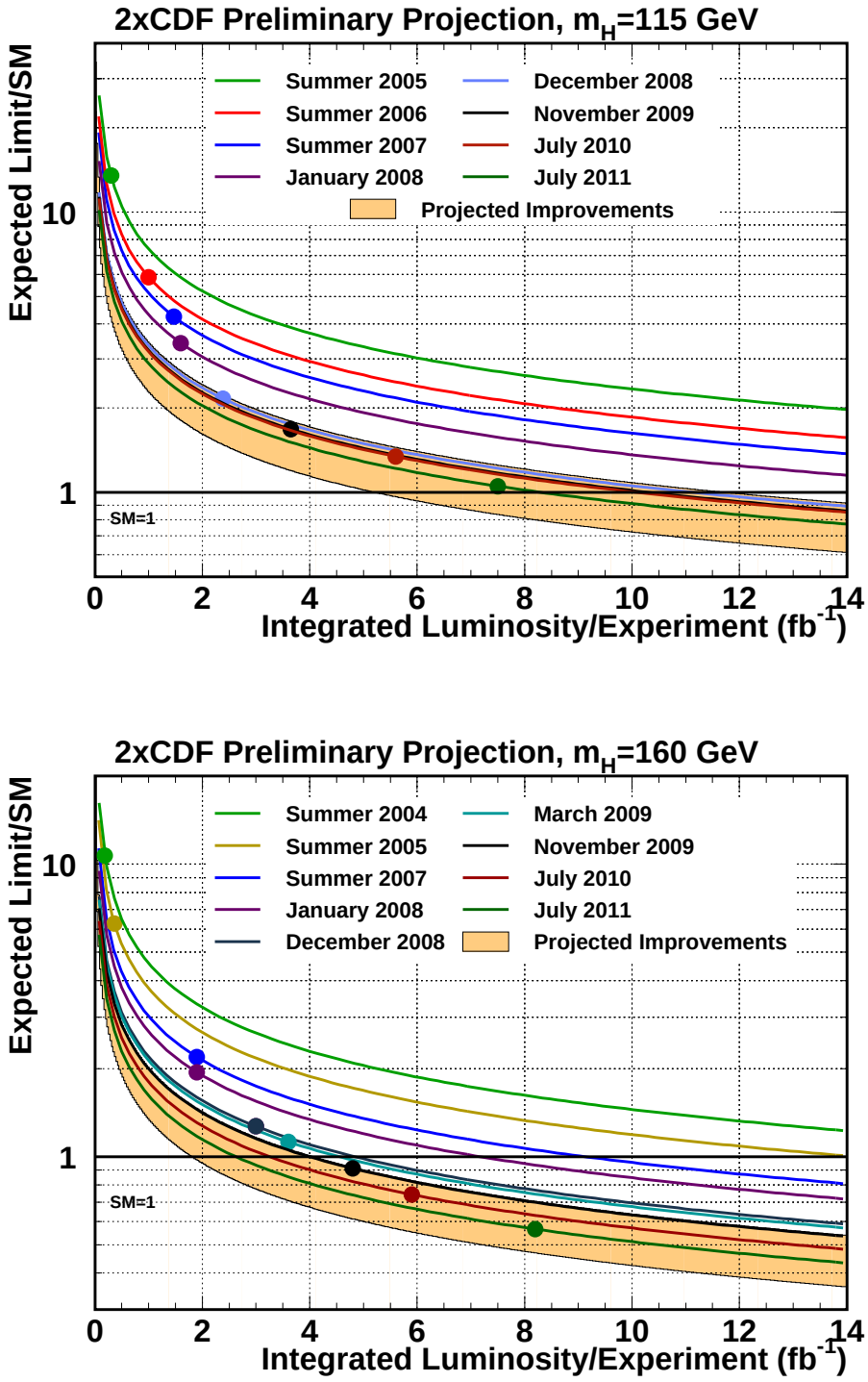


FIG. 7: Sensitivity projections and achieved sensitivities for the combined CDF Higgs boson searches, at $m_H = 115$ and 160 GeV/$c^2$, with a multiplier of $1/\sqrt{2}$ applied to the expected limits, to approximate the contribution of D0, assuming identical performance. The curves are proportional to $1/\sqrt{\int Ldt}$ extrapolations of the median expected limits, and each analysis update corresponds to a new point with a new curve. The light orange bands indicate ranges of possible improvements in performance, relative to the Summer 2007 sensitivity. The top of the light orange bands is a factor of 1.5 below the Summer 2007 curve, and the bottom of the light orange bands are a further factor of 1.5 below the top of the light orange bands. The points represent CDF's achieved sensitivities, where the expected limits have been divided by $\sqrt{2}$.

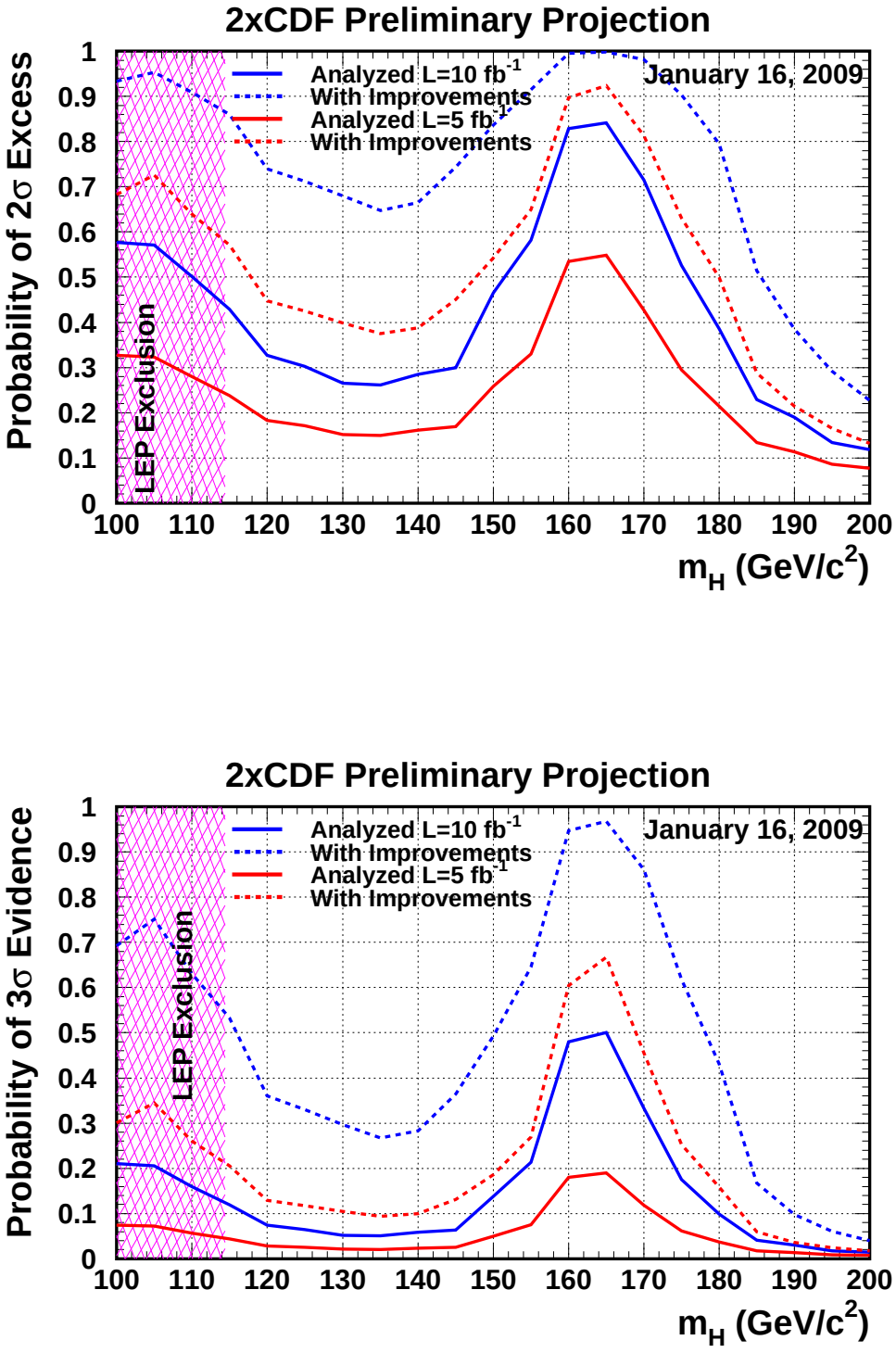


FIG. 8: Sensitivity projections as functions of $m_H$. These graphs show the chances of observing a $2\sigma$ excess (top) or a $3\sigma$ evidence (bottom), as functions of $m_H$, assuming a Higgs boson is present with production cross sections and decays at their SM values. CDF and D0 are assumed to contribute equally. The solid lines correspond to current performance as described in this note, and the dashed lines correspond to a performance level which corresponds to the bottom of the light orange bands in Figure 7. No account is taken of the data already collected and analyzed; existing excesses and deficits in the data do not affect these sensitivity projections. Two luminosity scenarios are considered: 5 fb$^{-1}$ of analyzed luminosity per experiment (red lines) and 10 fb$^{-1}$ of analyzed luminosity per experiment (blue lines).

[1] "Combined Upper Limits on Standard Model Higgs Boson Production from the D0 Experiment in up to 8.6 fb$^{-1}$ of data", D0 Conference Note 6xxx (2011).

[2] "Combined CDF and D0 Upper Limits on Standard Model Higgs Boson Production with up to 8.6 fb$^{-1}$ of Data", CDF Note 10606, D0 Note 6226 (2011).

[3] The CDF and D0 Collaborations and the TEVNPH Working Group, "Combined CDF and D0 Upper Limits on Standard Model Higgs Boson Production with up to 8.2 fb$^{-1}$ of Data,", FERMILAB-CONF-11-044-E, CDF Note 10441, D0 Note 6184, arXiv:1103.3233v1 [hep-ex] (2011);
The CDF and D0 Collaborations and the TEVNPH Working Group, "Combined CDF and D0 Upper Limits on Standard Model Higgs-Boson Production with up to 6.7 fb$^{-1}$ of Data", FERMILAB-CONF-10-257-E, CDF Note 10241, D0 Note 6096, arXiv:1007.4587v1 [hep-ex] (2010);
The CDF and D0 Collaborations and the TEVNPH Working Group, "Combined CDF and DZero Upper Limits on Standard Model Higgs-Boson Production with 2.1 to 4.2 fb$^{-1}$ of Data", FERMILAB-PUB-09-0557-E, CDF Note 9998, D0 Note 5983, arXiv:0911.3930v1 [hep-ex] (2009).
CDF Collaboration, "Search for $H \to WW^*$ Production Using 5.9 fb$^{-1}$", CDF Conference Note 10432 (2011);
CDF Collaboration, "Combined Upper Limit on Standard Model Higgs Boson Production for ICHEP 2010",CDF Conference Note 10241 (2010);
CDF Collaboration, "Combined Upper Limit on Standard Model Higgs Boson Production for HCP 2009", CDF Conference Note 9999 (2009);
CDF Collaboration, "Combined Upper Limit on Standard Model Higgs Boson Production for Summer 2009", CDF Conference Note 9807 (2009);

[4] CDF Collaboration, " Inclusive Search for Standard Model Higgs Boson Production in the WW Decay Channel Using the CDF II Detector", Phys. Rev. Lett. 104, 061803 (2010);
The CDF and D0 Collaborations, "Combination of Tevatron Searches for the Standard Model Higgs Boson in the $W^+W^-$ Decay Mode", Phys. Rev. Lett. 104, 061802 (2010).

[5] CDF Collaboration, "Search for standard model Higgs boson production in association with a $W$ boson with 7.5 fb$^{-1}$", CDF Conference Note 10596 (2011).

[6] CDF Collaboration, "Search for standard model Higgs boson production in association with a $W$ boson using Matrix Element techniques with 5.6 fb$^{-1}$ of CDF Data", CDF Conference Note 10217 (2010).

[7] CDF Collaboration, "Search for the standard model Higgs boson in the $\not\!\!E_T$ plus $b$-jets signature in 7.8 fb$^{-1}$", CDF Conference Note 10583 (2011).

[8] CDF Collaboration, "A Search for the standard model Higgs boson in the process $ZH \to e^+e^-b\bar{b}$ using 7.5 fb$^{-1}$ of CDF II Data", CDF Conference Note 10593 (2011).

[9] CDF Collaboration, "Search for the standard model Higgs boson in the $ZH \to \mu^+\mu^-b\bar{b}$ final state using 7.9 fb$^{-1}$", CDF Conference Note 10572 (2011).

[10] CDF Collaboration, "Search for $H \to WW^*$ Production Using 8.2 fb$^{-1}$", CDF Conference Note 10599 (2011).

[11] CDF Collaboration, "A search for the Higgs boson in the four lepton final state", CDF Conference Note 10573 (2011).

[12] CDF Collaboration, "Search for a low mass standard model Higgs boson in the di-tau decay channel using 6.0 fb$^{-1}$", CDF Conference Note 10439 (2011).

[13] CDF Collaboration, "Search for the standard model Higgs in the $\ell\nu\tau\tau$ and $\ell\ell\tau\tau$ channels", CDF Conference Note 10500 (2011).

[14] CDF Collaboration, "A search for the Higgs Boson in the All Hadronic Channel with Data Sample of 4 fb$^{-1}$", CDF Conference Note 10010 (2010).

[15] CDF Collaboration, "Search for a standard model Higgs boson decaying into photons at CDF using 6.0 fb$^{-1}$ of data", CDF Conference Note 10485 (2011).

[16] CDF Collaboration, "Search for the Higgs boson produced in association with top quarks", CDF Conference Note 10574 (2011).

[17] CDF Collaboration, "Search for standard model Higgs boson production in association with $t\bar{t}$ using no lepton final state", CDF Conference Note 10582 (2011).

[18] C. Anastasiou, G. Dissertori, M. Grazzini, F. Stöckli and B. R. Webber, JHEP **0908**, 099 (2009).

[19] C. Anastasiou, R. Boughezal and F. Petriello, JHEP **0904**, 003 (2009).

[20] D. de Florian and M. Grazzini, Phys. Lett. B **674**, 291 (2009).

[21] M. Grazzini, private communication (2010).

[22] The CDF and D0 Collaborations and the Tevatron Electroweak Working Group, arXiv:1007.3178 [hep-ex],

arXiv:0903.2503 [hep-ex].
[23] I. W. Stewart, F. J. Tackmann, [arXiv:1107.2117 [hep-ph]].
[24] J. M. Campbell, R. K. Ellis, C. Williams, Phys. Rev. **D81**, 074023 (2010). [arXiv:1001.4495 [hep-ph]].
[25] R. V. Harlander and W. B. Kilgore, Phys. Rev. Lett. **88**, 201801 (2002).
[26] C. Anastasiou and K. Melnikov, Nucl. Phys. B **646**, 220 (2002).
[27] V. Ravindran, J. Smith, and W. L. van Neerven, Nucl. Phys. B **665**, 325 (2003).
[28] S. Actis, G. Passarino, C. Sturm, and S. Uccirati, Phys. Lett. B **670**, 12 (2008).
[29] U. Aglietti, R. Bonciani, G. Degrassi, A. Vicini, "Two-loop electroweak corrections to Higgs production in proton-proton collisions", arXiv:hep-ph/0610033v1 (2006).
[30] S. Catani, D. de Florian, M. Grazzini and P. Nason, "Soft-gluon resummation for Higgs boson production at hadron colliders," JHEP **0307**, 028 (2003) [arXiv:hep-ph/0306211].
[31] A. D. Martin, W. J. Stirling, R. S. Thorne and G. Watt, Eur. Phys. J. C **63**, 189 (2009).
[32] `http://www.hep.ucl.ac.uk/pdf4lhc/`;
S. Alekhin *et al.*, (PDF4LHC Working Group), [arXiv:1101.0536v1 [hep-ph]];
M. Botje *et al.*, (PDF4LHC Working Group), [arXiv:1101.0538v1 [hep-ph]].
[33] P. M. Nadolsky *et al.*, Phys. Rev. D **78**, 013004 (2008) [arXiv:0802.0007 [hep-ph]].
[34] R. D. Ball *et al.* [NNPDF Collaboration], Nucl. Phys. B **809**, 1 (2009) [Erratum-ibid. B **816**, 293 (2009)] [arXiv:0808.1231 [hep-ph]].
[35] K. A. Assamagan *et al.* [Higgs Working Group Collaboration], "The Higgs working group: Summary report 2003," arXiv:hep-ph/0406152.
[36] O. Brein, A. Djouadi, and R. Harlander, Phys. Lett. B **579**, 149 (2004).
[37] M. L. Ciccolini, S. Dittmaier, and M. Kramer, Phys. Rev. D **68**, 073003 (2003).
[38] E. Berger and J. Campbell, Phys. Rev. D **70** 073011 (2004).
[39] W. Beenaker, S. Dittmaier, M. Krämer, B. Plümper, M. Spira, and P. M. Zerwas, Phys. Rev. Lett. **87**, 201805 (2001);
L. Reina and S. Dawson, Phys. Rev. Lett. **87**, 201804 (2001).
[40] J. Baglio and A. Djouadi, arXiv:1003.4266 [hep-ph] (2010). We have obtained extended versions of the table of $WH$ and $ZH$ cross sections for all Higgs boson masses we test, and with more digits of precision, from the authors.
[41] The Fortran program can be found on Michael Spira's web page `http://people.web.psi.ch/~mspira/proglist.html`.
[42] O. Brein, A. Djouadi, and R. Harlander, Phys. Lett. B **579**, 149 (2004).
[43] M. L. Ciccolini, S. Dittmaier, and M. Kramer, Phys. Rev. D **68**, 073003 (2003).
[44] P. Bolzoni, F. Maltoni, S.-O. Moch, and M. Zaro, Phys. Rev. Lett. **105**, 011801 (2010) [arXiv:1003.4451v2 [hep-ph]].
[45] M. Ciccolini, A. Denner, and S. Dittmaier, Phys. Rev. Lett. **99**, 161803 (2007) [arXiv:0707.0381 [hep-ph]];
M. Ciccolini, A. Denner, and S. Dittmaier, Phys. Rev. D **77**, 013002 (2008) [arXiv:0710.4749 [hep-ph]].
We would like to thank the authors of the HAWK program for adapting it to the Tevatron.
[46] T. Sjöstrand, L. Lonnblad and S. Mrenna, "PYTHIA 6.2: Physics and manual," arXiv:hep-ph/0108264.
[47] H. L. Lai *et al.*, Phys. Rev D **55**, 1280 (1997).
[48] S. Dittmaier *et al.* [ LHC Higgs Cross Section Working Group Collaboration ], [arXiv:1101.0593 [hep-ph]].
[49] A. Djouadi, J. Kalinowski and M. Spira, Comput. Phys. Commun. **108**, 56 (1998).
[50] A. Bredenstein, A. Denner, S. Dittmaier, and M. M. Weber, Phys. Rev. D **74**, 013004 (2006);
A. Bredenstein, A. Denner, S. Dittmaier, and M. Weber, JHEP **0702**, 080 (2007);
A. Bredenstein, A. Denner, S. Dittmaier, A. Mück, and M. M. Weber, JHEP **0702**, 080 (2007) `http://omnibus.uni-freiburg.de/~sd565/programs/prophycey4f/prophecy4f.html` (2010).
[51] J. Baglio, A. Djouadi, JHEP **1103**, 055 (2011). [arXiv:1012.0530 [hep-ph]].
[52] M. L. Mangano, M. Moretti, F. Piccinini, R. Pittau and A. D. Polosa, "ALPGEN, a generator for hard multiparton processes in hadronic collisions," JHEP **0307**, 001 (2003).
[53] S. Frixione and B.R. Webber, JHEP **0206**, 029 (2002).
[54] G. Corcella *et al.*, JHEP **0101**, 010 (2001).
[55] A. Pukhov *et al.*, "CompHEP: A package for evaluation of Feynman diagrams and integration over multi-particle phase space. User's manual for version 33," [arXiv:hep-ph/9908288].
[56] J. Campbell and R. K. Ellis, http://mcfm.fnal.gov/.
[57] T. Junk, Nucl. Instrum. Meth. A **434**, 435 (1999);
A.L. Read, "Modified Frequentist analysis of search results (the $CL_s$ method)", in F. James, L. Lyons and Y. Perrin (eds.), *Workshop on Confidence Limits*, CERN, Yellow Report 2000-005, available through `cdsweb.cern.ch`.
[58] W. Fisher, "Systematics and Limit Calculations," FERMILAB-TM-2386-E.
[59] S. Moch and P. Uwer, U. Langenfeld, S. Moch and P. Uwer, Phys. Rev. D **80**, 054009 (2009).
[60] The CDF and D0 Collaborations and the Tevatron Electroweak Working Group, arXiv:0903.2503 [hep-ex].

[61] M. Cacciari, S. Frixione, M. L. Mangano, P. Nason and G. Ridolfi, JHEP **0809**, 127 (2008).
N. Kidonakis and R. Vogt, Phys. Rev. D **78**, 074005 (2008).
[62] N. Kidonakis, Phys. Rev. D **74**, 114012 (2006).
[63] N. Kidonakis, private communication.
[64] N. Kidonakis, arXiv:1005.3330 [hep-ph].
[65] B. W. Harris, E. Laenen, L. Phaf, Z. Sullivan and S. Weinzierl, Phys. Rev. D **66**, 054024 (2002).
[66] J. Campbell and R. K. Ellis, Phys. Rev. D **65**, 113007 (2002).

# Appendices

## APPENDIX A: SYSTEMATIC UNCERTAINTIES

TABLE IV: Systematic uncertainties on the signal and background contributions for CDF's $WH \to \ell\nu b\bar{b}$ tight double tag (TDT), loose double tag (LDT), looser double tag (LDTX), and single tag (ST) 2 jet channels. Systematic uncertainties are listed by name; see the original references for a detailed explanation of their meaning and on how they are derived. Systematic uncertainties for $WH$ shown in this table are obtained for $m_H = 115$ GeV/$c^2$. Uncertainties are relative, in percent, and are symmetric unless otherwise indicated. Shape uncertainties are labeled with an "S".

CDF: tight and loose double-tag (TDT and LDT) $WH \to \ell\nu b\bar{b}$ channel relative uncertainties (%)

| Contribution | $W$+HF | Mistags | Top | Diboson | Non-$W$ | $WH$ |
|---|---|---|---|---|---|---|
| Luminosity ($\sigma_{\rm inel}(p\bar{p})$) | 3.8 | 0 | 3.8 | 3.8 | 0 | 3.8 |
| Luminosity Monitor | 4.4 | 0 | 4.4 | 4.4 | 0 | 4.4 |
| Lepton ID | 2.0-4.5 | 0 | 2.0-4.5 | 2.0-4.5 | 0 | 2.0-4.5 |
| Jet Energy Scale | S | 0 | S | S | 0 | 2(S) |
| Mistag Rate | 0 | 35 | 0 | 0 | 0 | 0 |
| $B$-Tag Efficiency | 8.6 | 0 | 8.6 | 8.6 | 0 | 8.6 |
| $t\bar{t}$ Cross Section | 0 | 0 | 10 | 0 | 0 | 0 |
| Diboson Rate | 0 | 0 | 0 | 11.5 | 0 | 0 |
| Signal Cross Section | 0 | 0 | 0 | 0 | 0 | 5 |
| HF Fraction in W+jets | 45 | 0 | 0 | 0 | 0 | 0 |
| ISR+FSR+PDF | 5.0-7.7 | 0 | 5.0-7.7 | 5.0-7.7 | 0 | 5.0-7.7 |
| $Q^2$ | S | 0 | 0 | 0 | 0 | 0 |
| QCD Rate | 0 | 0 | 0 | 0 | 40 | 0 |

CDF: looser double-tag (LDTX) $WH \to \ell\nu b\bar{b}$ channel relative uncertainties (%)

| Contribution | $W$+HF | Mistags | Top | Diboson | Non-$W$ | $WH$ |
|---|---|---|---|---|---|---|
| Luminosity ($\sigma_{\rm inel}(p\bar{p})$) | 3.8 | 0 | 3.8 | 3.8 | 0 | 3.8 |
| Luminosity Monitor | 4.4 | 0 | 4.4 | 4.4 | 0 | 4.4 |
| Lepton ID | 2.0-4.5 | 0 | 2.0-4.5 | 2.0-4.5 | 0 | 2.0-4.5 |
| Jet Energy Scale | S | | S | S | | 2.2(S) |
| Mistag Rate | 0 | 36 | 0 | 0 | 0 | 0 |
| $B$-Tag Efficiency | 13.6 | 0 | 13.6 | 13.6 | 0 | 13.6 |
| $t\bar{t}$ Cross Section | 0 | 0 | 10 | 0 | 0 | 0 |
| Diboson Rate | 0 | 0 | 0 | 11.5 | 0 | 0 |
| Signal Cross Section | 0 | 0 | 0 | 0 | 0 | 5 |
| HF Fraction in W+jets | 45 | 0 | 0 | 0 | 0 | 0 |
| ISR+FSR+PDF | 4.9-19.5 | 0 | 4.9-19.5 | 4.9-19.5 | 0 | 4.9-19.5 |
| $Q^2$ | S | 0 | 0 | 0 | 0 | 0 |
| QCD Rate | 0 | 0 | 0 | 0 | 40 | 0 |

CDF: single tag (ST) $WH \to \ell\nu b\bar{b}$ channel relative uncertainties (%)

| Contribution | $W$+HF | Mistags | Top | Diboson | Non-$W$ | $WH$ |
|---|---|---|---|---|---|---|
| Luminosity ($\sigma_{\rm inel}(p\bar{p})$) | 3.8 | 0 | 3.8 | 3.8 | 0 | 3.8 |
| Luminosity Monitor | 4.4 | 0 | 4.4 | 4.4 | 0 | 4.4 |
| Lepton ID | 2.0-4.5 | 0 | 2.0-4.5 | 2.0-4.5 | 0 | 2.0-4.5 |
| Jet Energy Scale | S | 0 | S | S | 0 | 2.3-4.7(S) |
| Mistag Rate | 0 | 35 | 0 | 0 | 0 | 0 |
| $B$-Tag Efficiency | 4.3 | 0 | 4.3 | 4.3 | 0 | 4.3 |
| $t\bar{t}$ Cross Section | 0 | 0 | 10 | 0 | 0 | 0 |
| Diboson Rate | 0 | 0 | 0 | 11.5 | 0 | 0 |
| Signal Cross Section | 0 | 0 | 0 | 0 | 0 | 5 |
| HF Fraction in W+jets | 42 | 0 | 0 | 0 | 0 | 0 |
| ISR+FSR+PDF | 3.0-8.4 | 0 | 3.0-8.4 | 3.0-8.4 | 0 | 3.0-8.4 |
| $Q^2$ | S | 0 | 0 | 0 | 0 | 0 |
| QCD Rate | 0 | 0 | 0 | 0 | 40 | 0 |

TABLE V: Systematic uncertainties on the signal and background contributions for CDF's $WH \to \ell\nu b\bar{b}$ tight double tag (TDT), loose double tag (LDT), and single tag (ST) 3 jet channels. Systematic uncertainties are listed by name; see the original references for a detailed explanation of their meaning and on how they are derived. Systematic uncertainties for $WH$ shown in this table are obtained for $m_H = 115$ GeV/$c^2$. Uncertainties are relative, in percent, and are symmetric unless otherwise indicated. Shape uncertainties are labeled with an "S".

CDF: tight and loose double-tag (TDT and LDT) $WH \to \ell\nu b\bar{b}$ channel relative uncertainties (%)

| Contribution | $W$+HF | Mistags | Top | Diboson | Non-$W$ | $WH$ |
|---|---|---|---|---|---|---|
| Luminosity ($\sigma_{\rm inel}(p\bar{p})$) | 3.8 | 0 | 3.8 | 3.8 | 0 | 3.8 |
| Luminosity Monitor | 4.4 | 0 | 4.4 | 4.4 | 0 | 4.4 |
| Lepton ID | 2 | 0 | 2 | 2 | 0 | 2 |
| Jet Energy Scale | S | 0 | S | 0 | 0 | 13.5(S) |
| Mistag Rate | 0 | 9 | 0 | 0 | 0 | 0 |
| $B$-Tag Efficiency | 8.4 | 0 | 8.4 | 8.4 | 0 | 8.4 |
| $t\bar{t}$ Cross Section | 0 | 0 | 10 | 0 | 0 | 0 |
| Diboson Rate | 0 | 0 | 0 | 10 | 0 | 0 |
| Signal Cross Section | 0 | 0 | 0 | 0 | 0 | 10 |
| HF Fraction in W+jets | 30 | 0 | 0 | 0 | 0 | 0 |
| ISR+FSR+PDF | 21.4 | 0 | 21.4 | 21.4 | 0 | 21.4 |
| QCD Rate | 0 | 0 | 0 | 0 | 40 | 0 |

CDF: single tag (ST) $WH \to \ell\nu b\bar{b}$ channel relative uncertainties (%)

| Contribution | $W$+HF | Mistags | Top | Diboson | Non-$W$ | $WH$ |
|---|---|---|---|---|---|---|
| Luminosity ($\sigma_{\rm inel}(p\bar{p})$) | 3.8 | 0 | 3.8 | 3.8 | 0 | 3.8 |
| Luminosity Monitor | 4.4 | 0 | 4.4 | 4.4 | 0 | 4.4 |
| Lepton ID | 2 | 0 | 2 | 2 | 0 | 2 |
| Jet Energy Scale | S | 0 | S | 0 | 0 | 15.8(S) |
| Mistag Rate | 0 | 13.3 | 0 | 0 | 0 | 0 |
| $B$-Tag Efficiency | 3.5 | 0 | 3.5 | 3.5 | 0 | 3.5 |
| $t\bar{t}$ Cross Section | 0 | 0 | 10 | 0 | 0 | 0 |
| Diboson Rate | 0 | 0 | 0 | 10 | 0 | 0 |
| Signal Cross Section | 0 | 0 | 0 | 0 | 0 | 10 |
| HF Fraction in W+jets | 30 | 0 | 0 | 0 | 0 | 0 |
| ISR+FSR+PDF | 13.1 | 0 | 13.1 | 13.1 | 0 | 13.1 |
| QCD Rate | 0 | 0 | 0 | 0 | 40 | 0 |

TABLE VI: Systematic uncertainties on the signal and background contributions for CDF's $WH, ZH \to \not\!\!E_T b\bar{b}$ tight double tag (TDT), loose double tag (LDT), and single tag (ST) channels. Systematic uncertainties are listed by name; see the original references for a detailed explanation of their meaning and on how they are derived. Systematic uncertainties for $ZH$ and $WH$ shown in this table are obtained for $m_H = 120$ GeV/$c^2$. Uncertainties are relative, in percent, and are symmetric unless otherwise indicated.

CDF: tight double-tag (TDT) $WH, ZH \to \not\!\!E_T b\bar{b}$ channel relative uncertainties (%)

| Contribution | ZH | WH | Multijet | Mistags | Top Pair | S. Top | Di-boson | W + h.f. | Z + h.f. |
|---|---|---|---|---|---|---|---|---|---|
| Luminosity | 3.8 | 3.8 | | | 3.8 | 3.8 | 3.8 | 3.8 | 3.8 |
| Lumi Monitor | 4.4 | 4.4 | | | 4.4 | 4.4 | 4.4 | 4.4 | 4.4 |
| Tagging SF | 10.4 | 10.4 | | | 10.4 | 10.4 | 10.4 | 10.4 | 10.4 |
| Trigger Eff. (shape) | 0.9 | 1.4 | 0.9 | | 0.9 | 1.6 | 2.0 | 1.8 | 1.2 |
| Lepton Veto | 2.0 | 2.0 | | | 2.0 | 2.0 | 2.0 | 2.0 | 2.0 |
| PDF Acceptance | 3.0 | 3.0 | | | 3.0 | 3.0 | 3.0 | 3.0 | 3.0 |
| JES (shape) | $^{+1.7}_{-1.8}$ | $^{+2.4}_{-2.3}$ | | | $^{+0.0}_{-0.1}$ | $^{+2.5}_{-2.4}$ | $^{+4.1}_{-4.5}$ | $^{+4.3}_{-4.6}$ | $^{+8.8}_{-3.2}$ |
| ISR/FSR | $^{+3.0}_{+3.0}$ | | | | | | | | |
| Cross-Section | 5 | 5 | | | 10 | 10 | 6 | 30 | 30 |
| Multijet Norm. (shape) | | | 2.5 | | | | | | |
| Mistag (shape) | | | | $^{+36.7}_{-30}$ | | | | | |

CDF: loose double-tag (LDT) $WH, ZH \to \not\!\!E_T b\bar{b}$ channel relative uncertainties (%)

| Contribution | ZH | WH | Multijet | Mistags | Top Pair | S. Top | Di-boson | W + h.f. | Z + h.f. |
|---|---|---|---|---|---|---|---|---|---|
| Luminosity | 3.8 | 3.8 | | | 3.8 | 3.8 | 3.8 | 3.8 | 3.8 |
| Lumi Monitor | 4.4 | 4.4 | | | 4.4 | 4.4 | 4.4 | 4.4 | 4.4 |
| Tagging SF | 8.3 | 8.3 | | | 8.3 | 8.3 | 8.3 | 8.3 | 8.3 |
| Trigger Eff. (shape) | 1.2 | 1.7 | 1.6 | | 0.9 | 1.8 | 2.0 | 2.5 | 1.9 |
| Lepton Veto | 2.0 | 2.0 | | | 2.0 | 2.0 | 2.0 | 2.0 | 2.0 |
| PDF Acceptance | 3.0 | 3.0 | | | 3.0 | 3.0 | 3.0 | 3.0 | 3.0 |
| JES (shape) | $^{+1.9}_{-1.9}$ | $^{+2.4}_{-2.4}$ | | | $^{+3.0}_{-2.8}$ | $^{-0.6}_{0.2}$ | $^{+4.2}_{-4.2}$ | $^{+6.8}_{-5.9}$ | $^{+8.3}_{-3.1}$ |
| ISR/FSR | $^{+2.4}_{-2.4}$ | | | | | | | | |
| Cross-Section | 5.0 | 5.0 | | | 10 | 10 | 6 | 30 | 30 |
| Multijet Norm. | | | 1.6 | | | | | | |
| Mistag (shape) | | | | $^{+65.2}_{-38.5}$ | | | | | |

CDF: single-tag (ST) $WH, ZH \to \not\!\!E_T b\bar{b}$ channel relative uncertainties (%)

| Contribution | ZH | WH | Multijet | Mistags | Top Pair | S. Top | Di-boson | W + h.f. | Z + h.f. |
|---|---|---|---|---|---|---|---|---|---|
| Luminosity | 3.8 | 3.8 | | | 3.8 | 3.8 | 3.8 | 3.8 | 3.8 |
| Lumi Monitor | 4.4 | 4.4 | | | 4.4 | 4.4 | 4.4 | 4.4 | 4.4 |
| Tagging SF | 5.2 | 5.2 | | | 5.2 | 5.2 | 5.2 | 5.2 | 5.2 |
| Trigger Eff. (shape) | 1.2 | 1.7 | 1.6 | | 0.9 | 1.8 | 2.0 | 2.5 | 1.9 |
| Lepton Veto | 2.0 | 2.0 | | | 2.0 | 2.0 | 2.0 | 2.0 | 2.0 |
| PDF Acceptance | 3.0 | 3.0 | | | 3.0 | 3.0 | 3.0 | 3.0 | 3.0 |
| JES (shape) | $^{+2.6}_{-2.6}$ | $^{+3.3}_{-3.1}$ | | | $^{-0.8}_{+0.6}$ | $^{+2.7}_{-2.8}$ | $^{+5.1}_{-5.1}$ | $^{+8.2}_{-6.8}$ | $^{+10.8}_{-3.4}$ |
| ISR/FSR | $^{+2.0}_{-2.0}$ | | | | | | | | |
| Cross-Section | 5.0 | 5.0 | | | 10 | 10 | 6 | 30 | 30 |
| Multijet Norm. | | | 0.7 | | | | | | |
| Mistag (shape) | | | | $^{+17.9}_{-17.4}$ | | | | | |

TABLE VII: Systematic uncertainties on the signal and background contributions for CDF's $ZH \to \mu^+\mu^- b\bar{b}$ single tag (ST), tight double tag (TDT), and loose double tag (LDT) channels. Systematic uncertainties are listed by name; see the original references for a detailed explanation of their meaning and on how they are derived. Systematic uncertainties for $ZH$ shown in this table are obtained for $m_H = 115$ GeV/$c^2$. Uncertainties are relative, in percent, and are symmetric unless otherwise indicated.

CDF: single tag (ST) $ZH \to \mu^+\mu^- b\bar{b}$ channel relative uncertainties (%)

| Contribution | Fakes | $t\bar{t}$ | $WW$ | $WZ$ | $ZZ$ | $Z + b\bar{b}$ | $Z + c\bar{c}$ | Mistags | $ZH$ |
|---|---|---|---|---|---|---|---|---|---|
| Luminosity ($\sigma_{\text{inel}}(p\bar{p})$) | | 3.8 | 3.8 | 3.8 | 3.8 | 3.8 | 3.8 | | 3.8 |
| Luminosity Monitor | | 4.4 | 4.4 | 4.4 | 4.4 | 4.4 | 4.4 | | 4.4 |
| Lepton ID | | 1 | 1 | 1 | 1 | 1 | 1 | | 1 |
| Lepton Energy Scale | | 1.5 | 1.5 | 1.5 | 1.5 | 1.5 | 1.5 | | 1.5 |
| Fake Leptons | 5 | | | | | | | | |
| Mistag Rate | | | | | | | | $^{+13.6}_{-13.7}$ | |
| Jet Energy Scale (shape dep.) | | $^{+1.8}_{-1.9}$ | $^{+18.7}_{-3.7}$ | $^{+3.9}_{-4.3}$ | $^{+4.3}_{-5.4}$ | $^{+7.9}_{-6.7}$ | $^{+7.9}_{-6.6}$ | | $^{+1.7}_{-2.6}$ |
| $b$-tag Rate | | 5.2 | 5.2 | 5.2 | 5.2 | 5.2 | 5.2 | | 5.2 |
| $t\bar{t}$ Cross Section | | 10 | | | | | | | |
| Diboson Cross Section | | | 6 | 6 | 6 | | | | |
| $Z$+HF Cross Section | | | | | | 40 | 40 | | |
| $ZH$ Cross Section | | | | | | | | | 5 |
| ISR/FSR | | | | | | | | | 1 |
| NN Trigger Model | | 5 | 5 | 5 | 5 | 5 | 5 | | 5 |

CDF: tight double tag (TDT) $ZH \to \mu^+\mu^- b\bar{b}$ channel relative uncertainties (%)

| Contribution | Fakes | $t\bar{t}$ | $WZ$ | $ZZ$ | $WW$ | $Z + b\bar{b}$ | $Z + c\bar{c}$ | Mistags | $ZH$ |
|---|---|---|---|---|---|---|---|---|---|
| Luminosity ($\sigma_{\text{inel}}(p\bar{p})$) | | 3.8 | 3.8 | 3.8 | 3.8 | 3.8 | 3.8 | | 3.8 |
| Luminosity Monitor | | 4.4 | 4.4 | 4.4 | 4.4 | 4.4 | 4.4 | | 4.4 |
| Lepton ID | | 1 | 1 | 1 | 1 | 1 | 1 | | 1 |
| Lepton Energy Scale | | 1.5 | 1.5 | 1.5 | 1.5 | 1.5 | 1.5 | | 1.5 |
| Fake Leptons | 5 | | | | | | | | |
| Mistag Rate | | | | | | | | $^{+28.7}_{-25.1}$ | |
| Jet Energy Scale (shape dep.) | | $^{+1.6}_{-1.7}$ | $^{+3.5}_{-3.7}$ | $^{+3.5}_{-3.7}$ | $^{+4.1}_{-4.4}$ | $^{+7.5}_{-3.8}$ | $^{+6.6}_{-5.2}$ | | $^{+1.4}_{-2.3}$ |
| $b$-tag Rate | | 10.2 | 10.2 | 10.2 | 10.2 | 10.2 | 10.2 | | 10.2 |
| $t\bar{t}$ Cross Section | | 10 | | | | | | | |
| Diboson Cross Section | | | 6 | 6 | 6 | | | | |
| $Z$+HF Cross Section | | | | | | 40 | 40 | | |
| $ZH$ Cross Section | | | | | | | | | 5 |
| ISR/FSR | | | | | | | | | 5 |
| NN Trigger Model | | 5 | 5 | 5 | 5 | 5 | 5 | | 5 |

CDF: loose double tag (LDT) $ZH \to \mu^+\mu^- b\bar{b}$ channel relative uncertainties (%)

| Contribution | Fakes | $t\bar{t}$ | $WW$ | $WZ$ | $ZZ$ | $Z + b\bar{b}$ | $Z + c\bar{c}$ | Mistags | $ZH$ |
|---|---|---|---|---|---|---|---|---|---|
| Luminosity ($\sigma_{\rm inel}(p\bar{p})$) | | 3.8 | 3.8 | 3.8 | 3.8 | 3.8 | 3.8 | | 3.8 |
| Luminosity Monitor | | 4.4 | 4.4 | 4.4 | 4.4 | 4.4 | 4.4 | | 4.4 |
| Lepton ID | | 1 | 1 | 1 | 1 | 1 | 1 | | 1 |
| Lepton Energy Scale | | 1.5 | 1.5 | 1.5 | 1.5 | 1.5 | 1.5 | | 1.5 |
| Fake Leptons | 5 | | | | | | | | |
| Mistag Rate | | | | | | | | $^{+27.2}_{-24.0}$ | |
| Jet Energy Scale (shape dep.) | | $^{+1.6}_{-1.8}$ | $^{+3.5}_{-3.7}$ | $^{+4.6}_{-7.6}$ | $^{+4.0}_{-4.2}$ | $^{+6.9}_{-5.9}$ | $^{+7.8}_{-5.9}$ | | $^{+1.5}_{-2.4}$ |
| $b$-tag Rate | | 8.7 | 8.7 | 8.7 | 8.7 | 8.7 | 8.7 | | 8.7 |
| $t\bar{t}$ Cross Section | | 10 | | | | | | | |
| Diboson Cross Section | | | 6 | 6 | 6 | | | | |
| $Z$+HF Cross Section | | | | | | 40 | 40 | | |
| $ZH$ Cross Section | | | | | | | | | 5 |
| ISR/FSR | | | | | | | | | 2 |
| NN Trigger Model | | 5 | 5 | 5 | 5 | 5 | 5 | | 5 |

TABLE VIII: Systematic uncertainties on the signal and background contributions for CDF's $ZH \to e^+e^- b\bar{b}$ single tag (ST), tight double tag (TDT), and loose double tag (LDT) channels. Systematic uncertainties are listed by name; see the original references for a detailed explanation of their meaning and on how they are derived. Systematic uncertainties for $ZH$ shown in this table are obtained for $m_H = 115$ GeV/$c^2$. Uncertainties are relative, in percent, and are symmetric unless otherwise indicated.

CDF: single tag (ST) $ZH \to e^+e^- b\bar{b}$ channel relative uncertainties (%)

| Contribution | Fakes | Top | $WW$ | $WZ$ | $ZZ$ | $Z + b\bar{b}$ | $Z + c\bar{c}$ | $Z$+l.f. | $ZH$ |
|---|---|---|---|---|---|---|---|---|---|
| Luminosity ($\sigma_{\rm inel}(p\bar{p})$) | 0 | 3.8 | 3.8 | 3.8 | 3.8 | 3.8 | 3.8 | 0 | 3.8 |
| Luminosity Monitor | 0 | 4.4 | 4.4 | 4.4 | 4.4 | 4.4 | 4.4 | 0 | 4.4 |
| Trigger Emulation | 0 | 1 | 1 | 1 | 1 | 1 | 1 | 0 | 1 |
| Lepton ID | 0 | 2 | 2 | 2 | 2 | 2 | 2 | 0 | 2 |
| Lepton Energy Scale | 0 | 3 | 3 | 3 | 3 | 3 | 3 | 0 | 3 |
| $ZH$ Cross Section | 0 | 0 | 0 | 0 | 0 | 0 | 0 | 0 | 5 |
| Fake Leptons | 50 | 0 | 0 | 0 | 0 | 0 | 0 | 0 | 0 |
| B-Tag Efficiency | 0 | 5.2 | 5.2 | 5.2 | 5.2 | 5.2 | 5.2 | 0 | 5.2 |
| $t\bar{t}$ Cross Section | 0 | 10 | 0 | 0 | 0 | 0 | 0 | 0 | 0 |
| Diboson Cross Section | 0 | 0 | 6 | 6 | 6 | 0 | 0 | 0 | 0 |
| $\sigma(p\bar{p} \to Z + HF)$ | 0 | 0 | 0 | 0 | 40 | 40 | 40 | 0 | 0 |
| ISR/FSR | 0 | 0 | 0 | 0 | 0 | 0 | 0 | 0 | 4.0 |
| Mistag Rate (shape dep.) | 0 | 0 | 0 | 0 | 0 | 0 | 0 | $^{+13.9}_{-13.8}$ | 0 |
| Jet Energy Scale (shape dep.) | 0 | $^{+1.9}_{-2.5}$ | $^{+19.6}_{-4.0}$ | $^{+5.2}_{-6.2}$ | $^{+5.3}_{-7.1}$ | $^{+12.1}_{-11.1}$ | $^{+4.1}_{-9.9}$ | 0 | $^{+3.0}_{-4.3}$ |

CDF: tight double tag (TDT) $ZH \to e^+e^-b\bar{b}$ channel relative uncertainties (%)

| Contribution | Fakes | Top | $WZ$ | $ZZ$ | $Z+b\bar{b}$ | $Z+c\bar{c}$ | $Z$+l.f. | $ZH$ |
|---|---|---|---|---|---|---|---|---|
| Luminosity ($\sigma_{\rm inel}(p\bar{p})$) | 0 | 3.8 | 3.8 | 3.8 | 3.8 | 3.8 | 0 | 3.8 |
| Luminosity Monitor | 0 | 4.4 | 4.4 | 4.4 | 4.4 | 4.4 | 0 | 4.4 |
| Trigger Emulation | 0 | 1 | 1 | 1 | 1 | 1 | 0 | 1 |
| Lepton ID | 0 | 2 | 2 | 2 | 2 | 2 | 0 | 2 |
| Lepton Energy Scale | 0 | 3 | 3 | 3 | 3 | 3 | 0 | 3 |
| $ZH$ Cross Section | 0 | 0 | 0 | 0 | 0 | 0 | 0 | 5 |
| Fake Leptons | 50 | 0 | 0 | 0 | 0 | 0 | 0 | 0 |
| B-Tag Efficiency | 0 | 10.4 | 10.4 | 10.4 | 10.4 | 10.4 | 0 | 10.4 |
| $t\bar{t}$ Cross Section | 0 | 10 | 0 | 0 | 0 | 0 | 0 | 0 |
| Diboson Cross Section | 0 | 0 | 6 | 6 | 0 | 0 | 0 | 0 |
| $\sigma(p\bar{p} \to Z+HF)$ | 0 | 0 | 0 | 40 | 40 | 40 | 0 | 0 |
| ISR/FSR | 0 | 0 | 0 | 0 | 0 | 0 | 0 | 4.0 |
| Mistag Rate (shape dep.) | 0 | 0 | 0 | 0 | 0 | 0 | $^{+29.3}_{-25.4}$ | 0 |
| Jet Energy Scale (shape dep.) | 0 | $^{+1.4}_{-2.6}$ | $^{+7.8}_{-3.1}$ | $^{+3.4}_{-5.9}$ | $^{+6.8}_{-6.6}$ | $^{+1.0}_{-3.7}$ | 0 | $^{+1.6}_{-2.7}$ |

CDF: loose double tag (LDT) $ZH \to e^+e^-b\bar{b}$ channel relative uncertainties (%)

| Contribution | Fakes | Top | $WW$ | $WZ$ | $ZZ$ | $Z+b\bar{b}$ | $Z+c\bar{c}$ | $Z$+l.f. | $ZH$ |
|---|---|---|---|---|---|---|---|---|---|
| Luminosity ($\sigma_{\rm inel}(p\bar{p})$) | 0 | 3.8 | 3.8 | 3.8 | 3.8 | 3.8 | 3.8 | 0 | 3.8 |
| Luminosity Monitor | 0 | 4.4 | 4.4 | 4.4 | 4.4 | 4.4 | 4.4 | 0 | 4.4 |
| Trigger Emulation | 0 | 1 | 1 | 1 | 1 | 1 | 1 | 0 | 1 |
| Lepton ID | 0 | 2 | 2 | 2 | 2 | 2 | 2 | 0 | 2 |
| Lepton Energy Scale | 0 | 3 | 3 | 3 | 3 | 3 | 3 | 0 | 3 |
| $ZH$ Cross Section | 0 | 0 | 0 | 0 | 0 | 0 | 0 | 0 | 5 |
| Fake Leptons | 50 | 0 | 0 | 0 | 0 | 0 | 0 | 0 | 0 |
| B-Tag Efficiency | 0 | 8.7 | 8.7 | 8.7 | 8.7 | 8.7 | 8.7 | 0 | 8.7 |
| $t\bar{t}$ Cross Section | 0 | 10 | 0 | 0 | 0 | 0 | 0 | 0 | 0 |
| Diboson Cross Section | 0 | 0 | 6 | 6 | 6 | 0 | 0 | 0 | 0 |
| $\sigma(p\bar{p} \to Z+HF)$ | 0 | 0 | 0 | 0 | 40 | 40 | 40 | 0 | 0 |
| ISR/FSR | 0 | 0 | 0 | 0 | 0 | 0 | 0 | 0 | 4.0 |
| Mistag Rate (shape dep.) | 0 | 0 | 0 | 0 | 0 | 0 | 0 | $^{+25.5}_{-21.4}$ | 0 |
| Jet Energy Scale (shape dep.) | 0 | $^{+1.3}_{-2.3}$ | 0 | $^{+7.5}_{-0.1}$ | $^{+4.1}_{-4.4}$ | $^{+8.2}_{-7.8}$ | $^{+3.3}_{-5.5}$ | 0 | $^{+2.1}_{-2.7}$ |

TABLE IX: Systematic uncertainties on the signal and background contributions for CDF's $H \to W^+W^- \to \ell^\pm\ell'^\mp$ channels with zero, one, and two or more associated jets. These channels are sensitive to gluon fusion production (all channels) and $WH, ZH$ and VBF production. Systematic uncertainties are listed by name (see the original references for a detailed explanation of their meaning and on how they are derived). Systematic uncertainties for $H$ shown in this table are obtained for $m_H = 160$ GeV/$c^2$. Uncertainties are relative, in percent, and are symmetric unless otherwise indicated. The uncertainties associated with the different background and signal processed are correlated within individual jet categories unless otherwise noted. Boldface and italics indicate groups of uncertainties which are correlated with each other but not the others on the line.

CDF: $H \to W^+W^- \to \ell^\pm\ell'^\mp$ with no associated jet channel relative uncertainties (%)

| Contribution | $WW$ | $WZ$ | $ZZ$ | $t\bar{t}$ | DY | $W\gamma$ | $W$+jet | $gg \to H$ | $WH$ | $ZH$ | VBF |
|---|---|---|---|---|---|---|---|---|---|---|---|
| **Cross Section :** | | | | | | | | | | | |
| Scale (Inclusive) | | | | | | | | 13.4 | | | |
| Scale (1+ Jets) | | | | | | | | -23.0 | | | |
| Scale (2+ Jets) | | | | | | | | 0.0 | | | |
| PDF Model | | | | | | | | 7.6 | | | |
| Total | *6.0* | *6.0* | *6.0* | 7.0 | | | | | **5.0** | **5.0** | 10.0 |
| **Acceptance :** | | | | | | | | | | | |
| Scale (jets) | *0.3* | | | | | | | | | | |
| PDF Model (leptons) | | | | | | | | 2.7 | | | |
| PDF Model (jets) | *1.1* | | | | | | | 5.5 | | | |
| Higher-order Diagrams | | *10.0* | *10.0* | 10.0 | | 10.0 | | | **10.0** | **10.0** | **10.0** |
| $\not\!\!E_T$ Modeling | | | | | 19.5 | | | | | | |
| Conversion Modeling | | | | | | 10.0 | | | | | |
| Jet Fake Rates | | | | | | | | | | | |
| (Low S/B) | | | | | | | 22.0 | | | | |
| (High S/B) | | | | | | | 26.0 | | | | |
| Jet Energy Scale | *2.6* | *6.1* | *3.4* | *26.0* | *17.5* | *3.1* | | *5.0* | *10.5* | *5.0* | *11.5* |
| Lepton ID Efficiencies | *3.8* | *3.8* | *3.8* | *3.8* | *3.8* | | | *3.8* | *3.8* | *3.8* | *3.8* |
| Trigger Efficiencies | *2.0* | *2.0* | *2.0* | *2.0* | *2.0* | | | *2.0* | *2.0* | *2.0* | *2.0* |
| **Luminosity** | *3.8* | *3.8* | *3.8* | *3.8* | *3.8* | | | *3.8* | *3.8* | *3.8* | *3.8* |
| **Luminosity Monitor** | *4.4* | *4.4* | *4.4* | *4.4* | *4.4* | | | *4.4* | *4.4* | *4.4* | *4.4* |

CDF: $H \to W^+W^- \to \ell^\pm\ell'^\mp$ with one associated jet channel relative uncertainties (%)

| Contribution | $WW$ | $WZ$ | $ZZ$ | $t\bar{t}$ | DY | $W\gamma$ | $W$+jet | $gg \to H$ | $WH$ | $ZH$ | VBF |
|---|---|---|---|---|---|---|---|---|---|---|---|
| **Cross Section :** | | | | | | | | | | | |
| Scale (Inclusive) | | | | | | | | 0.0 | | | |
| Scale (1+ Jets) | | | | | | | | 35.0 | | | |
| Scale (2+ Jets) | | | | | | | | -12.7 | | | |
| PDF Model | | | | | | | | 17.3 | | | |
| Total | *6.0* | *6.0* | *6.0* | 7.0 | | | | | **5.0** | **5.0** | 10.0 |
| **Acceptance :** | | | | | | | | | | | |
| Scale (jets) | *-4.0* | | | | | | | | | | |
| PDF Model (leptons) | | | | | | | | *3.6* | | | |
| PDF Model (jets) | *4.7* | | | | | | | -6.3 | | | |
| Higher-order Diagrams | | *10.0* | *10.0* | 10.0 | | 10.0 | | | **10.0** | **10.0** | **10.0** |
| $\not\!\!E_T$ Modeling | | | | | 20.0 | | | | | | |
| Conversion Modeling | | | | | | 10.0 | | | | | |
| Jet Fake Rates | | | | | | | | | | | |
| (Low S/B) | | | | | | | 23.0 | | | | |
| (High S/B) | | | | | | | 29.0 | | | | |
| Jet Energy Scale | *-5.5* | *-1.0* | *-4.3* | *-13.0* | *-6.5* | *-9.5* | | *-4.0* | *-8.5* | *-7.0* | *-6.5* |
| Lepton ID Efficiencies | *3.8* | *3.8* | *3.8* | *3.8* | *3.8* | | | *3.8* | *3.8* | *3.8* | *3.8* |
| Trigger Efficiencies | *2.0* | *2.0* | *2.0* | *2.0* | *2.0* | | | *2.0* | *2.0* | *2.0* | *2.0* |
| **Luminosity** | *3.8* | *3.8* | *3.8* | *3.8* | *3.8* | | | *3.8* | *3.8* | *3.8* | *3.8* |
| **Luminosity Monitor** | *4.4* | *4.4* | *4.4* | *4.4* | *4.4* | | | *4.4* | *4.4* | *4.4* | *4.4* |

CDF: $H \to W^+W^- \to \ell^\pm\ell'^\mp$ with two or more associated jets channel relative uncertainties (%)

| Contribution | $WW$ | $WZ$ | $ZZ$ | $t\bar{t}$ | DY | $W\gamma$ | $W$+jet | $gg \to H$ | $WH$ | $ZH$ | VBF |
|---|---|---|---|---|---|---|---|---|---|---|---|
| **Cross Section :** | | | | | | | | | | | |
| Scale (Inclusive) | | | | | | | | 0.0 | | | |
| Scale (1+ Jets) | | | | | | | | 0.0 | | | |
| Scale (2+ Jets) | | | | | | | | 33.0 | | | |
| PDF Model | | | | | | | | 29.7 | | | |
| Total | *6.0* | *6.0* | *6.0* | 7.0 | | | | | **5.0** | **5.0** | 10.0 |
| **Acceptance :** | | | | | | | | | | | |
| Scale (jets) | *-8.2* | | | | | | | | | | |
| PDF Model (leptons) | | | | | | | | *4.8* | | | |
| PDF Model (jets) | *4.2* | | | | | | | -12.3 | | | |
| Higher-order Diagrams | | *10.0* | *10.0* | 10.0 | | 10.0 | | | **10.0** | **10.0** | **10.0** |
| $\not\!\!E_T$ Modeling | | | | | 25.5 | | | | | | |
| Conversion Modeling | | | | | | 10.0 | | | | | |
| Jet Fake Rates | | | | | | | 28.0 | | | | |
| Jet Energy Scale | *-14.8* | *-12.9* | *-12.1* | *-1.7* | *-29.2* | *-22.0* | | *-17.0* | *-4.0* | *-2.3* | *-4.0* |
| $b$-tag Veto | | | | 3.8 | | | | | | | |
| Lepton ID Efficiencies | *3.8* | *3.8* | *3.8* | *3.8* | *3.8* | | | *3.8* | *3.8* | *3.8* | *3.8* |
| Trigger Efficiencies | *2.0* | *2.0* | *2.0* | *2.0* | *2.0* | | | *2.0* | *2.0* | *2.0* | *2.0* |
| **Luminosity** | *3.8* | *3.8* | *3.8* | *3.8* | *3.8* | | | *3.8* | *3.8* | *3.8* | *3.8* |
| **Luminosity Monitor** | *4.4* | *4.4* | *4.4* | *4.4* | *4.4* | | | *4.4* | *4.4* | *4.4* | *4.4* |

TABLE X: Systematic uncertainties on the signal and background contributions for CDF's low-$M_{\ell\ell}$ $H \to W^+W^- \to \ell^\pm\ell'^\mp$ channel with zero or one associated jets. This channel is sensitive to only gluon fusion production. Systematic uncertainties are listed by name (see the original references for a detailed explanation of their meaning and on how they are derived). Systematic uncertainties for $H$ shown in this table are obtained for $m_H = 160$ GeV/$c^2$. Uncertainties are relative, in percent, and are symmetric unless otherwise indicated. The uncertainties associated with the different background and signal processed are correlated within individual categories unless otherwise noted. In these special cases, the correlated uncertainties are shown in either italics or bold face text.

CDF: low $M_{\ell\ell}$ $H \to W^+W^- \to \ell^\pm\ell'^\mp$ with zero or one associated jets channel relative uncertainties (%)

| Contribution | $WW$ | $WZ$ | $ZZ$ | $t\bar{t}$ | DY | $W\gamma$ | $W$+jet(s) | $gg \to H$ | $WH$ | $ZH$ | VBF |
|---|---|---|---|---|---|---|---|---|---|---|---|
| **Cross Section :** | | | | | | | | | | | |
| Scale (Inclusive) | | | | | | | | 8.1 | | | |
| Scale (1+ Jets) | | | | | | | | 0.0 | | | |
| Scale (2+ Jets) | | | | | | | | -5.1 | | | |
| PDF Model | | | | | | | | 10.5 | | | |
| Total | *6.0* | *6.0* | *6.0* | 7.0 | 5.0 | | | | **5.0** | **5.0** | 10.0 |
| **Acceptance :** | | | | | | | | | | | |
| Scale (jets) | *-0.4* | | | | | | | | | | |
| PDF Model (leptons) | | | | | | | | *1.0* | | | |
| PDF Model (jets) | *1.6* | | | | | | | 2.1 | | | |
| Higher-order Diagrams | | *10.0* | *10.0* | 10.0 | 10.0 | | | | **10.0** | **10.0** | **10.0** |
| Jet Energy Scale | *1.1* | *2.2* | *2.0* | *13.5* | *6.4* | *1.3* | | *2.4* | *9.2* | *6.5* | *7.8* |
| Conversion Modeling | | | | | | 10.0 | | | | | |
| Boson Radiation Model | | | | | 25.0 | | | | | | |
| Jet Fake Rates | | | | | | | 13.5 | | | | |
| Lepton ID Efficiencies | *3.8* | *3.8* | *3.8* | *3.8* | *3.8* | | | *3.8* | *3.8* | *3.8* | *3.8* |
| Trigger Efficiencies | *2.0* | *2.0* | *2.0* | *2.0* | *2.0* | | | *2.0* | *2.0* | *2.0* | *2.0* |
| **Luminosity** | *3.8* | *3.8* | *3.8* | *3.8* | *3.8* | | | *3.8* | *3.8* | *3.8* | *3.8* |
| **Luminosity Monitor** | *4.4* | *4.4* | *4.4* | *4.4* | *4.4* | | | *4.4* | *4.4* | *4.4* | *4.4* |

TABLE XI: Systematic uncertainties on the signal and background contributions for CDF's $H \to W^+W^- \to e^\pm\tau^\mp$ and $H \to W^+W^- \to \mu^\pm\tau^\mp$ channels. These channels are sensitive to gluon fusion production, $WH, ZH$ and VBF production. Systematic uncertainties are listed by name (see the original references for a detailed explanation of their meaning and on how they are derived). Systematic uncertainties for $H$ shown in this table are obtained for $m_H = 160$ GeV/$c^2$. Uncertainties are relative, in percent, and are symmetric unless otherwise indicated. The uncertainties associated with the different background and signal processed are correlated within individual categories unless otherwise noted. In these special cases, the correlated uncertainties are shown in either italics or bold face text.

CDF: $H \to W^+W^- \to e^\pm\tau^\mp$ channel relative uncertainties ( )

| Contribution | $WW$ | $WZ$ | $ZZ$ | $t\bar{t}$ | $Z \to \tau\tau$ | $Z \to \ell\ell$ | $W$+jet | $W\gamma$ | $gg \to H$ | $WH$ | $ZH$ | VBF |
|---|---|---|---|---|---|---|---|---|---|---|---|---|
| Cross section | 6.0 | 6.0 | 6.0 | 10.0 | 5.0 | 5.0 | | | 10.3 | 5 | 5 | 10 |
| Measured W cross-section | | | | | | | 12 | | | | | |
| PDF Model | 1.6 | 2.3 | 3.2 | 2.3 | 2.7 | 4.6 | 2.2 | 3.1 | 2.5 | 2.0 | 1.9 | 1.8 |
| Higher order diagrams | 10 | 10 | 10 | 10 | 10 | 10 | | 10 | | 10 | 10 | 10 |
| Conversion modeling | | | | | | | | 10 | | | | |
| Trigger Efficiency | 0.5 | 0.6 | 0.6 | 0.6 | 0.7 | 0.5 | 0.6 | 0.6 | 0.5 | 0.5 | 0.6 | 0.5 |
| Lepton ID Efficiency | 0.4 | 0.5 | 0.5 | 0.4 | 0.4 | 0.4 | 0.5 | 0.4 | 0.4 | 0.4 | 0.4 | 0.4 |
| $\tau$ ID Efficiency | 1.0 | 1.3 | 1.9 | 1.3 | 2.1 | | | 0.3 | 2.8 | 1.6 | 1.7 | 2.8 |
| Jet into $\tau$ Fake rate | 5.8 | 4.8 | 2.0 | 5.1 | | 0.1 | 8.8 | | | 4.2 | 4.0 | 0.4 |
| Lepton into $\tau$ Fake rate | 0.2 | 0.1 | 0.6 | 0.2 | | 2.3 | | 2.1 | 0.15 | 0.06 | 0.15 | 0.11 |
| W+jet scale | | | | | | | 1.6 | | | | | |
| MC Run dependence | 2.6 | 2.6 | 2.6 | | | | 2.6 | | | | | |
| Luminosity | 3.8 | 3.8 | 3.8 | 3.8 | 3.8 | 3.8 | 3.8 | 3.8 | 3.8 | 3.8 | 3.8 | 3.8 |
| Luminosity Monitor | 4.4 | 4.4 | 4.4 | 4.4 | 4.4 | 4.4 | 4.4 | 4.4 | 4.4 | 4.4 | 4.4 | 4.4 |

CDF: $H \to W^+W^- \to \mu^\pm\tau^\mp$ channel relative uncertainties (%)

| Contribution | $WW$ | $WZ$ | $ZZ$ | $t\bar{t}$ | $Z \to \tau\tau$ | $Z \to \ell\ell$ | $W$+jet | $W\gamma$ | $gg \to H$ | $WH$ | $ZH$ | VBF |
|---|---|---|---|---|---|---|---|---|---|---|---|---|
| Cross section | 6.0 | 6.0 | 6.0 | 10.0 | 5.0 | 5.0 | | | 10.4 | 5 | 5 | 10 |
| Measured W cross-section | | | | | | | 12 | | | | | |
| PDF Model | 1.5 | 2.1 | 2.9 | 2.1 | 2.5 | 4.3 | 2.0 | 2.9 | 2.6 | 2.2 | 2.0 | 2.2 |
| Higher order diagrams | 10 | 10 | 10 | 10 | | | | 11 | | 10 | 10 | 10 |
| Trigger Efficiency | 1.3 | 0.7 | 0.7 | 1.1 | 0.9 | 1.3 | 1.0 | 1.0 | 1.3 | 1.3 | 1.2 | 1.3 |
| Lepton ID Efficiency | 1.1 | 1.4 | 1.4 | 1.1 | 1.2 | 1.1 | 1.4 | 1.3 | 1.0 | 1.0 | 1.0 | 1.0 |
| $\tau$ ID Efficiency | 1.0 | 1.2 | 1.4 | 1.6 | 1.9 | | | | 2.9 | 1.6 | 1.7 | 2.8 |
| Jet into $\tau$ Fake rate | 5.8 | 5.0 | 4.4 | 4.4 | | 0.2 | 8.8 | | | 4.5 | 4.2 | 0.4 |
| Lepton into $\tau$ Fake rate | 0.06 | 0.05 | 0.09 | 0.04 | | 1.9 | | 1.2 | 0.04 | 0.02 | 0.02 | 0.04 |
| W+jet scale | | | | | | | 1.4 | | | | | |
| MC Run dependence | 3.0 | 3.0 | 3.0 | | | | 3.0 | | | | | |
| Luminosity | 3.8 | 3.8 | 3.8 | 3.8 | 3.8 | 3.8 | 3.8 | 3.8 | 3.8 | 3.8 | 3.8 | 3.8 |
| Luminosity Monitor | 4.4 | 4.4 | 4.4 | 4.4 | 4.4 | 4.4 | 4.4 | 4.4 | 4.4 | 4.4 | 4.4 | 4.4 |

TABLE XII: Systematic uncertainties on the signal and background contributions for CDF's $WH \to WWW \to \ell^{\pm}\ell'^{\pm}$ channel with one or more associated jets and $WH \to WWW \to \ell^{\pm}\ell'^{\pm}\ell''^{\mp}$ channel. These channels are sensitive to only $WH$ and $ZH$ production. Systematic uncertainties are listed by name (see the original references for a detailed explanation of their meaning and on how they are derived). Systematic uncertainties for $H$ shown in this table are obtained for $m_H = 160$ GeV/$c^2$. Uncertainties are relative, in percent, and are symmetric unless otherwise indicated. The uncertainties associated with the different background and signal processed are correlated within individual categories unless otherwise noted. In these special cases, the correlated uncertainties are shown in either italics or bold face text.

CDF: $WH \to WWW \to \ell^{\pm}\ell'^{\pm}$ channel relative uncertainties (%)

| Contribution | $WW$ | $WZ$ | $ZZ$ | $t\bar{t}$ | DY | $W\gamma$ | $W$+jet | $WH$ | $ZH$ |
|---|---|---|---|---|---|---|---|---|---|
| **Cross Section** | *6.0* | *6.0* | *6.0* | 7.0 | 5.0 | | | **5.0** | **5.0** |
| Scale (Acceptance) | *-6.1* | | | | | | | | |
| PDF Model (Acceptance) | *5.7* | | | | | | | | |
| Higher-order Diagrams | | *10.0* | *10.0* | 10.0 | 10.0 | 10.0 | | **10.0** | **10.0** |
| Conversion Modeling | | | | | | 10.0 | | | |
| Jet Fake Rates | | | | | | | 38.5 | | |
| Jet Energy Scale | *-14.0* | *-3.9* | *-2.8* | *-0.6* | *-7.7* | *-7.6* | | *-1.0* | *-0.7* |
| Charge Mismeasurement Rate | *40.0* | | | | *40.0* | | | | |
| Lepton ID Efficiencies | *3.8* | *3.8* | *3.8* | *3.8* | *3.8* | | | *3.8* | *3.8* |
| Trigger Efficiencies | *2.0* | *2.0* | *2.0* | *2.0* | *2.0* | | | *2.0* | *2.0* |
| **Luminosity** | *3.8* | *3.8* | *3.8* | *3.8* | *3.8* | | | *3.8* | *3.8* |
| **Luminosity Monitor** | *4.4* | *4.4* | *4.4* | *4.4* | *4.4* | | | *4.4* | *4.4* |

CDF: $WH \to WWW \to \ell^{\pm}\ell'^{\pm}\ell''^{\mp}$ channel relative uncertainties (%)

| Contribution | $WZ$ | $ZZ$ | $Z\gamma$ | $t\bar{t}$ | Fakes | $WH$ | $ZH$ |
|---|---|---|---|---|---|---|---|
| **Cross Section** | *6.0* | *6.0* | 10.0 | 7.0 | | **5.0** | **5.0** |
| Higher-order Diagrams | *10.0* | *10.0* | 15.0 | 10.0 | | **10.0** | **10.0** |
| Jet Energy Scale | | | *-2.7* | | | | |
| Jet Fake Rates | | | | | 25.6 | | |
| $b$-Jet Fake Rates | | | | 27.3 | | | |
| MC Run Dependence | | | 5.0 | | | | |
| Lepton ID Efficiencies | *5.0* | *5.0* | | *5.0* | | *5.0* | *5.0* |
| Trigger Efficiencies | *2.0* | *2.0* | | *2.0* | | *2.0* | *2.0* |
| **Luminosity** | *3.8* | *3.8* | | *3.8* | | *3.8* | *3.8* |
| **Luminosity Monitor** | *4.4* | *4.4* | | *4.4* | | *4.4* | *4.4* |

TABLE XIII: Systematic uncertainties on the signal and background contributions for CDF's $ZH \to ZWW \to \ell^{\pm}\ell^{\mp}\ell'^{\pm}$ channels with 1 jet and 2 or more jets. These channels are sensitive to only $WH$ and $ZH$ production. Systematic uncertainties are listed by name (see the original references for a detailed explanation of their meaning and on how they are derived). Systematic uncertainties for $H$ shown in this table are obtained for $m_H = 160$ GeV/$c^2$. Uncertainties are relative, in percent, and are symmetric unless otherwise indicated. The uncertainties associated with the different background and signal processed are correlated within individual categories unless otherwise noted. In these special cases, the correlated uncertainties are shown in either italics or bold face text.

CDF: $ZH \to ZWW \to \ell^{\pm}\ell^{\mp}\ell'^{\pm}$ with one associated jet channel relative uncertainties (%)

| Contribution | $WZ$ | $ZZ$ | $Z\gamma$ | $t\bar{t}$ | Fakes | $WH$ | $ZH$ |
|---|---|---|---|---|---|---|---|
| **Cross Section** | *6.0* | *6.0* | 10.0 | 7.0 | | **5.0** | **5.0** |
| Higher-order Diagrams | *10.0* | *10.0* | 15.0 | 10.0 | | **10.0** | **10.0** |
| Jet Energy Scale | *-7.6* | *-2.3* | *-5.3* | *9.4* | | *-9.0* | *8.1* |
| Jet Fake Rates | | | | | 24.8 | | |
| $b$-Jet Fake Rates | | | | 42.0 | | | |
| MC Run Dependence | | | 5.0 | | | | |
| Lepton ID Efficiencies | *5.0* | *5.0* | | *5.0* | | *5.0* | *5.0* |
| Trigger Efficiencies | *2.0* | *2.0* | | *2.0* | | *2.0* | *2.0* |
| **Luminosity** | *3.8* | *3.8* | | *3.8* | | *3.8* | *3.8* |
| **Luminosity Monitor** | *4.4* | *4.4* | | *4.4* | | *4.4* | *4.4%* |

CDF: $ZH \to ZWW \to \ell^{\pm}\ell^{\mp}\ell'^{\pm}$ with two or more associated jets channel relative uncertainties (%)

| Contribution | $WZ$ | $ZZ$ | $Z\gamma$ | $t\bar{t}$ | Fakes | $WH$ | $ZH$ |
|---|---|---|---|---|---|---|---|
| **Cross Section** | *6.0* | *6.0* | 10.0 | 7.0 | | **5.0** | **5.0** |
| Higher-order Diagrams | *10.0* | *10.0* | 15.0 | 10.0 | | **10.0** | **10.0** |
| Jet Energy Scale | *-17.8* | *-13.1* | *-18.2* | *-3.6* | | *-15.4* | *-4.9* |
| Jet Fake Rates | | | | | 25.6 | | |
| $b$-Jet Fake Rates | | | | 22.2 | | | |
| MC Run Dependence | | | 5.0 | | | | |
| Lepton ID Efficiencies | *5.0* | *5.0* | | *5.0* | | *5.0* | *5.0* |
| Trigger Efficiencies | *2.0* | *2.0* | | *2.0* | | *2.0* | *2.0* |
| **Luminosity** | *3.8* | *3.8* | | *3.8* | | *3.8* | *3.8* |
| **Luminosity Monitor** | *4.4* | *4.4* | | *4.4* | | *4.4* | *4.4* |

TABLE XIV: Systematic uncertainties on the signal and background contributions for CDF's $H \to \ell^{\pm}\ell^{\mp}\ell'^{\pm}\ell'^{\mp}$ channel. This channel is sensitive to gluon fusion production and $WH$, $ZH$ and VBF production. Systematic uncertainties are listed by name (see the original references for a detailed explanation of their meaning and on how they are derived). Uncertainties are relative, in percent, and are symmetric unless otherwise indicated. The uncertainties associated with the different background and signal processed are correlated unless otherwise noted. Boldface and italics indicate groups of uncertainties which are correlated with each other but not the others on the line.

CDF: $H \to \ell^{\pm}\ell^{\mp}\ell'^{\pm}\ell'^{\mp}$ channel relative uncertainties (%)

| Contribution | $ZZ$ | $Z(/\gamma^*)$+jets | $gg \to H$ | $WH$ | $ZH$ | VBF |
|---|---|---|---|---|---|---|
| **Cross Section :** | | | | | | |
| Scale | | | 7.0 | | | |
| PDF Model | | | 7.7 | | | |
| Total | *10.0* | | | **5.0** | **5.0** | 10.0 |
| $\mathcal{BR}(H \to VV)$ | | | 3.0 | 3.0 | 3.0 | 3.0 |
| **Acceptance :** | | | | | | |
| PDF Model | 2.7 | | | | | |
| Higher-order Diagrams | 2.5 | | | | | |
| Jet Fake Rates | | 50.0 | | | | |
| Lepton ID Efficiencies | *3.6* | | *3.6* | *3.6* | *3.6* | *3.6* |
| Trigger Efficiencies | *0.4* | | *0.4* | *0.4* | *0.4* | *0.4* |
| **Luminosity** | *3.8* | | *3.8* | *3.8* | *3.8* | *3.8* |
| **Luminosity Monitor** | *4.4* | | *4.4* | *4.4* | *4.4* | *4.4* |

TABLE XV: Systematic uncertainties on the signal and background contributions for CDF's $t\bar{t}H \to \ell$+jets channels. Systematic uncertainties are listed by name; see the original references for a detailed explanation of their meaning and on how they are derived. Systematic uncertainties for $t\bar{t}H$ shown in this table are obtained for $m_H = 115$ GeV/$c^2$. Uncertainties are relative, in percent, and are symmetric unless otherwise indicated.

CDF: $t\bar{t}H$ $\ell + \not\!\!E_T$+4 jets relative uncertainties (%)

| | 1 tight, 1 loose | | 1 tight, $\geq$ 2 loose | | 2 tight, 0 loose | | 2 tight, $\geq$ 1 loose | | $\geq$ 3 tight, $\geq$ 0 loose | |
|---|---|---|---|---|---|---|---|---|---|---|
| Contribution | $t\bar{t}$ | $t\bar{t}H$ | $t\bar{t}$ | $t\bar{t}H$ | $t\bar{t}$ | $t\bar{t}H$ | $t\bar{t}$ | $t\bar{t}H$ | $t\bar{t}$ | $t\bar{t}H$ |
| $t\bar{t}$ Cross Section | | 10 | | 10 | | 10 | | 10 | | 10 |
| $t\bar{t}H$ Cross Section | 10 | | 10 | | 10 | | 10 | | 10 | |
| Luminosity ($\sigma_{\text{inel}}(p\bar{p})$) | 3.8 | 3.8 | 3.8 | 3.8 | 3.8 | 3.8 | 3.8 | 3.8 | 3.8 | 3.8 |
| Luminosity Monitor | 4.4 | 4.4 | 4.4 | 4.4 | 4.4 | 4.4 | 4.4 | 4.4 | 4.4 | 4.4 |
| $B$-Tag Efficiency | $^{+1.4}_{-2.5}$ | $^{-2.9}_{-2.0}$ | $^{+3.3}_{-1.5}$ | $^{+0.3}_{+0.3}$ | $^{+7.3}_{-9.4}$ | $^{+6.7}_{-2.0}$ | $^{+8.3}_{-8.8}$ | $^{+7.0}_{-7.7}$ | $^{+11}_{-12}$ | $^{+11}_{-16}$ |
| Mistag Rate | $^{+1.7}_{-2.0}$ | $^{-0.4}_{-1.5}$ | $^{+10}_{-11}$ | $^{-1.1}_{-5.7}$ | $^{-1.2}_{+2.7}$ | $^{+2.7}_{+3.7}$ | $^{+7.6}_{-7.4}$ | $^{+1.7}_{+2.4}$ | $^{+3.3}_{-5.1}$ | $^{+1.6}_{+0.2}$ |
| Jet Energy Scale | $^{+3.8}_{-5.1}$ | $^{-13}_{+6.7}$ | $^{+2.5}_{-4.5}$ | $^{0.0}_{0.0}$ | $^{+4.2}_{-4.8}$ | $^{-5.9}_{+5.9}$ | $^{+2.5}_{-3.8}$ | $^{-12}_{0.0}$ | $^{+3.3}_{-4.4}$ | $^{-12}_{0.0}$ |
| ISR+FSR+PDF | $^{-1.8}_{-1.0}$ | $^{-0.1}_{+0.1}$ | $^{-1.3}_{+2.3}$ | $^{-0.5}_{+0.5}$ | $^{-3.8}_{-1.3}$ | $^{+0.2}_{-0.2}$ | $^{-4.4}_{-1.1}$ | $^{+0.0}_{-0.0}$ | $^{-2.9}_{-3.5}$ | $^{-0.2}_{+0.2}$ |

CDF: $t\bar{t}H$ $\ell + \not\!\!E_T$+5 jets relative uncertainties (%)

| | 1 tight, 1 loose | | 1 tight, $\geq$ 2 loose | | 2 tight, 0 loose | | 2 tight, $\geq$ 1 loose | | $\geq$ 3 tight, $\geq$ 0 loose | |
|---|---|---|---|---|---|---|---|---|---|---|
| Contribution | $t\bar{t}$ | $t\bar{t}H$ | $t\bar{t}$ | $t\bar{t}H$ | $t\bar{t}$ | $t\bar{t}H$ | $t\bar{t}$ | $t\bar{t}H$ | $t\bar{t}$ | $t\bar{t}H$ |
| $t\bar{t}$ Cross Section | | 10 | | 10 | | 10 | | 10 | | 10 |
| $t\bar{t}H$ Cross Section | 10 | | 10 | | 10 | | 10 | | 10 | |
| Luminosity ($\sigma_{\text{inel}}(p\bar{p})$) | 3.8 | 3.8 | 3.8 | 3.8 | 3.8 | 3.8 | 3.8 | 3.8 | 3.8 | 3.8 |
| Luminosity Monitor | 4.4 | 4.4 | 4.4 | 4.4 | 4.4 | 4.4 | 4.4 | 4.4 | 4.4 | 4.4 |
| $B$-Tag Efficiency | $^{+1.8}_{-3.5}$ | $^{-0.4}_{+2.7}$ | $^{+4.5}_{-4.1}$ | $^{-1.3}_{-1.6}$ | $^{+8.2}_{-6.8}$ | $^{+2.5}_{-5.0}$ | $^{+9.7}_{-7.7}$ | $^{+5.9}_{-5.5}$ | $^{+11}_{-16}$ | $^{+9.9}_{-13}$ |
| Mistag Rate | $^{+1.3}_{-2.9}$ | $^{-7.5}_{+1.8}$ | $^{+18}_{-8.9}$ | $^{+4.3}_{-6.6}$ | $^{-0.2}_{+2.6}$ | $^{-2.0}_{+1.0}$ | $^{+8.2}_{-8.7}$ | $^{+2.5}_{-2.2}$ | $^{+8.1}_{-3.4}$ | $^{+1.3}_{-0.5}$ |
| Jet Energy Scale | $^{+19}_{-16}$ | $^{+7.5}_{-7.5}$ | $^{+17}_{-15}$ | $^{+7.1}_{-14}$ | $^{+18}_{-17}$ | $^{+7.0}_{-4.7}$ | $^{+16}_{-16}$ | $^{+6.7}_{-3.3}$ | $^{+15}_{-15}$ | $^{-2.7}_{-8.1}$ |
| ISR+FSR+PDF | $^{+10}_{-1.2}$ | $^{-0.0}_{+0.0}$ | $^{+14}_{-1.0}$ | $^{-0.2}_{+0.2}$ | $^{+8.2}_{-6.5}$ | $^{+0.0}_{-0.0}$ | $^{+12}_{-5.1}$ | $^{-2.1}_{+2.1}$ | $^{+14}_{-2.0}$ | $^{-1.9}_{+1.9}$ |

TABLE XVI: Systematic uncertainties on the signal and background contributions for CDF's $t\bar{t}H$ 2-tag and 3-tag $\not\!\!E_T$+jets channels. Systematic uncertainties are listed by name; see the original references for a detailed explanation of their meaning and on how they are derived. Systematic uncertainties for $t\bar{t}H$ shown in this table are obtained for $m_H = 120$ GeV/$c^2$. Uncertainties are relative, in percent, and are symmetric unless otherwise indicated.

CDF: $t\bar{t}H$ $\not\!\!E_T$+jets 2-tag channel relative uncertainties (%)

| Contribution | non-$t\bar{t}$ | $t\bar{t}$ | $t\bar{t}H$ |
|---|---|---|---|
| Luminosity ($\sigma_{\rm inel}(p\bar{p})$) | 0 | 3.8 | 3.8 |
| Luminosity Monitor | 0 | 4.4 | 4.4 |
| Jet Energy Scale | 0 | 2 | 11 |
| Trigger Efficiency | 0 | 7 | 7 |
| $B$-Tag Efficiency | 0 | 7 | 7 |
| ISR/FSR | 0 | 2 | 2 |
| PDF | 0 | 2 | 2 |
| $t\bar{t}$ Cross Section | 0 | 10 | 0 |
| $t\bar{t}b\bar{b}$ Cross Section | 0 | 3 | 0 |
| Signal Cross Section | 0 | 0 | 10 |
| Background Modeling | 6 | 0 | 0 |
| Background $B$-tagging | 5 | 0 | 0 |

CDF: $t\bar{t}H$ $\not\!\!E_T$+jets 3-tag channel relative uncertainties (%)

| Contribution | non-$t\bar{t}$ | $t\bar{t}$ | $t\bar{t}H$ |
|---|---|---|---|
| Luminosity ($\sigma_{\rm inel}(p\bar{p})$) | 0 | 3.8 | 3.8 |
| Luminosity Monitor | 0 | 4.4 | 4.4 |
| Jet Energy Scale | 0 | 3 | 13 |
| Trigger Efficiency | 0 | 7 | 7 |
| $B$-Tag Efficiency | 0 | 9 | 9 |
| ISR/FSR | 0 | 2 | 2 |
| PDF | 0 | 2 | 2 |
| $t\bar{t}$ Cross Section | 0 | 10 | 0 |
| $t\bar{t}b\bar{b}$ Cross Section | 0 | 5 | 0 |
| Signal Cross Section | 0 | 0 | 10 |
| Background Modeling | 6 | 0 | 0 |
| Background $B$-tagging | 10 | 0 | 0 |

TABLE XVII: Systematic uncertainties on the signal and background contributions for CDF's $t\bar{t}H$ 2-tag and 3-tag all jets channels. Systematic uncertainties are listed by name; see the original references for a detailed explanation of their meaning and on how they are derived. Systematic uncertainties for $t\bar{t}H$ shown in this table are obtained for $m_H = 120$ GeV/$c^2$. Uncertainties are relative, in percent, and are symmetric unless otherwise indicated.

CDF: $t\bar{t}H$ all jets 2-tag channel relative uncertainties (%)

| Contribution | non-$t\bar{t}$ | $t\bar{t}$ | $t\bar{t}H$ |
|---|---|---|---|
| Luminosity ($\sigma_{\rm inel}(p\bar{p})$) | 0 | 3.8 | 3.8 |
| Luminosity Monitor | 0 | 4.4 | 4.4 |
| Jet Energy Scale | 0 | 11 | 20 |
| Trigger Efficiency | 0 | 7 | 7 |
| $B$-Tag Efficiency | 0 | 7 | 7 |
| ISR/FSR | 0 | 2 | 2 |
| PDF | 0 | 2 | 2 |
| $t\bar{t}$ Cross Section | 0 | 10 | 0 |
| $t\bar{t}b\bar{b}$ Cross Section | 0 | 3 | 0 |
| Signal Cross Section | 0 | 0 | 10 |
| Background Modeling | 9 | 0 | 0 |
| Background $B$-tagging | 5 | 0 | 0 |

CDF: $t\bar{t}H$ all jets 3-tag channel relative uncertainties (%)

| Contribution | non-$t\bar{t}$ | $t\bar{t}$ | $t\bar{t}H$ |
|---|---|---|---|
| Luminosity ($\sigma_{\rm inel}(p\bar{p})$) | 0 | 3.8 | 3.8 |
| Luminosity Monitor | 0 | 4.4 | 4.4 |
| Jet Energy Scale | 0 | 13 | 22 |
| Trigger Efficiency | 0 | 7 | 7 |
| $B$-Tag Efficiency | 0 | 9 | 9 |
| ISR/FSR | 0 | 2 | 2 |
| PDF | 0 | 2 | 2 |
| $t\bar{t}$ Cross Section | 0 | 10 | 0 |
| $t\bar{t}b\bar{b}$ Cross Section | 0 | 6 | 0 |
| Signal Cross Section | 0 | 0 | 10 |
| Background Modeling | 9 | 0 | 0 |
| Background $B$-tagging | 10 | 0 | 0 |

TABLE XVIII: Systematic uncertainties on the signal and background contributions for CDF's $H \to \tau^+\tau^-$ channels. Systematic uncertainties are listed by name; see the original references for a detailed explanation of their meaning and on how they are derived. Systematic uncertainties for the Higgs signal shown in these tables are obtained for $m_H = 120$ GeV/$c^2$. Uncertainties are relative, in percent, and are symmetric unless otherwise indicated.

CDF: $H \to \tau^+\tau^-$ channel relative uncertainties (%)

| Contribution | $Z/\gamma^* \to \tau\tau$ | $Z/\gamma^* \to ee$ | $Z/\gamma^* \to \mu\mu$ | $t\bar{t}$ | diboson | fakes from SS | W+jets | $WH$ | $ZH$ | VBF | $gg \to H$ |
|---|---|---|---|---|---|---|---|---|---|---|---|
| PDF Uncertainty | 1 | 1 | 1 | 1 | 1 | - | - | 1.2 | 0.9 | 2.2 | 4.9 |
| ISR 1 JET | - | - | - | - | - | - | - | -6.9 | -2.9 | -1.8 | 11.8 |
| ISR $\geq$ 2 JETS | - | - | - | - | - | - | - | -0.5 | 0.1 | -1.9 | 18.1 |
| FSR 1 JET | - | - | - | - | - | - | - | 4.3 | 0.7 | 1.1 | -3.4 |
| FSR $\geq$ 2 JETS | - | - | - | - | - | - | - | -0.9 | -0.5 | -1.0 | -5.0 |
| JES (shape) 1 JET | 7.9 | 7.6 | 3.9 | -8.4 | 6.3 | - | - | -4.8 | -5.3 | -3.7 | 5.1 |
| JES (shape) $\geq$ 2 JETS | 14.0 | 11.0 | 20.1 | 2.8 | 11.7 | - | - | 5.4 | 4.8 | -5.2 | 13.2 |
| Normalization 1 JET | 2.2 | 2.2 | 2.2 | 10 | 6 | 10 | 25 | 5 | 5 | 10 | 23.5 |
| Normalization $\geq$2 JETS | 2.2 | 2.2 | 2.2 | 10 | 6 | 10 | 30 | 5 | 5 | 10 | 67.5 |
| MC Acceptance | 2.3 | 2.3 | 2.3 | - | - | - | - | - | - | - | - |
| $\varepsilon_{trig}$ (e/$\mu$ leg) | - | 0.3 | 1.0 | - | - | - | - | - | - | - | - |
| $\varepsilon_{trig}$ ($\tau$ leg) | - | 3.0 | 3.0 | - | - | - | - | - | - | - | - |
| $\varepsilon_{ID}lep$ | - | 2.4 | 2.6 | - | - | - | - | - | - | - | - |
| $\varepsilon_{vtx}$ | - | 0.5 | 0.5 | - | - | - | - | - | - | - | - |
| e/$\mu \to \tau_h$ fake rate | - | 7.4 | 15.5 | - | - | - | - | - | - | - | - |
| Luminosity | - | 5.9 | 5.9 | - | - | - | - | - | - | - | - |
| tau ID scale factor: | | | | | | | | | | | |
| $N_{obs}$ | 1.8 | - | - | 1.8 | 1.8 | - | - | 1.8 | 1.8 | 1.8 | 1.8 |
| $N_{SSdata}$ | -3.7 | - | - | -3.7 | -3.7 | - | - | -3.7 | -3.7 | -3.7 | -3.7 |
| $N_{W+jets}$ | -1.6 | - | - | -1.6 | -1.6 | - | - | -1.6 | -1.6 | -1.6 | -1.6 |
| Cross section (DY) | -2.1 | - | - | -2.1 | -2.1 | - | - | -2.1 | -2.1 | -2.1 | -2.1 |
| MC Acceptance (DY) | -2.2 | - | - | -2.2 | -2.2 | - | - | -2.2 | -2.2 | -2.2 | -2.2 |
| e/$\mu \to \tau_h$ fake rate | -0.1 | - | - | -0.1 | -0.1 | - | - | -0.1 | -0.1 | -0.1 | -0.1 |

TABLE XIX: Systematic uncertainties on the signal and background contributions for CDF's $WH \to \ell\nu\tau^+\tau^-$ and $ZH \to \ell^+\ell^-\tau^+\tau^-$ channels. Systematic uncertainties are listed by name; see the original references for a detailed explanation of their meaning and on how they are derived. Systematic uncertainties for the Higgs signal shown in these tables are obtained for $m_H = 120$ GeV/$c^2$. Uncertainties are relative, in percent, and are symmetric unless otherwise indicated.

CDF: $WH \to \ell\nu\tau^+\tau^-$ and $ZH \to \ell^+\ell^-\tau^+\tau^-$ $\ell\ell\tau_h + X$ channel relative uncertainties (%)

| Contribution | $ZZ$ | $WZ$ | $WW$ | $DY(ee)$ | $DY(\mu\mu)$ | $DY(\tau\tau)$ | $Z\gamma$ | $t\bar{t}$ | $W\gamma$ | $W+jet$ | $WH$ | $ZH$ | $VBF$ | $gg \to H$ |
|---|---|---|---|---|---|---|---|---|---|---|---|---|---|---|
| Luminosity | 5.9 | 5.9 | 5.9 | 5.9 | 5.9 | 5.9 | 5.9 | 5.9 | 5.9 | 5.9 | 5.9 | 5.9 | 5.9 | 5.9 |
| Cross Section | 11.7 | 11.7 | 11.7 | 5.0 | 5.0 | 5.0 | 11.7 | 14.1 | 11.7 | 5.0 | 5.0 | 5.0 | 10.0 | 10.0 |
| Z-vertex Cut Efficiency | 0.5 | 0.5 | 0.5 | 0.5 | 0.5 | 0.5 | 0.5 | 0.5 | 0.5 | 0.5 | 0.5 | 0.5 | 0.5 | 0.5 |
| Trigger Efficiency | 1.1 | 1.1 | 1.0 | 1.0 | 1.0 | 1.1 | 1.1 | 1.0 | 0.8 | 1.0 | 1.2 | 1.2 | 1.2 | 1.1 |
| Lepton ID Efficiency | 2.4 | 2.3 | 2.4 | 2.4 | 2.4 | 2.4 | 2.4 | 2.4 | 2.3 | 2.4 | 2.4 | 2.4 | 2.4 | 2.4 |
| Lepton Fake Rate | 10.7 | 8.0 | 26.7 | 26.0 | 26.6 | 15.1 | 27.1 | 22.4 | 22.8 | 28.7 | 2.9 | 2.3 | 15.1 | 13.6 |
| Jet Energy Scale | 1.3 | 1.1 | 0.0 | 3.2 | 5.1 | 0.6 | 6.6 | 0.1 | 2.0 | 0.2 | 0.1 | 0.03 | 0.6 | 0.4 |
| MC stat | 3.7 | 2.9 | 7.6 | 1.5 | 1.7 | 2.2 | 4.1 | 3.1 | 20.0 | 3.1 | 1.5 | 1.4 | 3.8 | 9.4 |
| PDF Model | - | - | - | - | - | - | - | - | - | - | 1.2 | 0.9 | 2.2 | 4.9 |
| ISR/FSR Uncertainties | - | - | - | - | - | - | - | - | - | - | 1.3 | 2.1 | 0.6 | 0.2 |

CDF: $WH \to \ell\nu\tau^+\tau^-$ and $ZH \to \ell^+\ell^-\tau^+\tau^-$ $e\mu\tau_h + X$ channel relative uncertainties (%)

| Contribution | $ZZ$ | $WZ$ | $WW$ | $DY(ee)$ | $DY(\mu\mu)$ | $DY(\tau\tau)$ | $Z\gamma$ | $t\bar{t}$ | $W\gamma$ | $W+jet$ | $WH$ | $ZH$ | $VBF$ | $gg \to H$ |
|---|---|---|---|---|---|---|---|---|---|---|---|---|---|---|
| Luminosity | 5.9 | 5.9 | 5.9 | 5.9 | 5.9 | 5.9 | 5.9 | 5.9 | 5.9 | 5.9 | 5.9 | 5.9 | 5.9 | 5.9 |
| Cross Section | 11.7 | 11.7 | 11.7 | 5.0 | 5.0 | 5.0 | 11.7 | 14.1 | 11.7 | 5.0 | 5.0 | 5.0 | 10.0 | 10.0 |
| Z-vertex Cut Efficiency | 0.5 | 0.5 | 0.5 | 0.5 | 0.5 | 0.5 | 0.5 | 0.5 | 0.5 | 0.5 | 0.5 | 0.5 | 0.5 | 0.5 |
| Trigger Efficiency | 1.4 | 1.4 | 1.1 | 1.1 | 1.3 | 1.1 | 1.4 | 1.1 | 1.0 | 0.7 | 1.3 | 1.3 | 1.2 | 1.2 |
| Lepton ID Efficiency | 2.4 | 2.4 | 2.4 | 2.4 | 2.4 | 2.4 | 2.4 | 2.4 | 2.4 | 2.4 | 2.4 | 2.4 | 2.4 | 2.4 |
| Lepton Fake Rate | 9.0 | 6.5 | 26.6 | 20.8 | 31.4 | 25.2 | 39.4 | 27.8 | 19.3 | 41.9 | 1.6 | 2.5 | 28.5 | 29.2 |
| Jet Energy Scale | 0.0 | 0.3 | 2.2 | 0.0 | 0.8 | 1.5 | 0.5 | 0.8 | 0.0 | 0.0 | 0.2 | 0.1 | 1.7 | 0.0 |
| MC stat | 12.9 | 7.2 | 20.9 | 57.7 | 12.6 | 7.7 | 10.2 | 12.4 | 35.4 | 25.8 | 2.1 | 3.9 | 13.0 | 44.7 |
| PDF Model | - | - | - | - | - | - | - | - | - | - | 1.2 | 0.9 | 2.2 | 4.9 |
| ISR/FSR Uncertainties | - | - | - | - | - | - | - | - | - | - | 0.6 | 0.2 | 0.1 | 0.0 |

CDF: $WH \to \ell\nu\tau^+\tau^-$ and $ZH \to \ell^+\ell^-\tau^+\tau^-$ $\ell\tau_h\tau_h + X$ channel relative uncertainties (%)

| Contribution | $ZZ$ | $WZ$ | $WW$ | $DY(ee)$ | $DY(\mu\mu)$ | $DY(\tau\tau)$ | $Z\gamma$ | $t\bar{t}$ | $W\gamma$ | $W+jet$ | $WH$ | $ZH$ | $VBF$ | $gg \to H$ |
|---|---|---|---|---|---|---|---|---|---|---|---|---|---|---|
| Luminosity | 5.9 | 5.9 | 5.9 | 5.9 | 5.9 | 5.9 | 5.9 | 5.9 | 5.9 | 5.9 | 5.9 | 5.9 | 5.9 | 5.9 |
| Cross Section | 11.7 | 11.7 | 11.7 | 5.0 | 5.0 | 5.0 | 11.7 | 14.1 | 11.7 | 5.0 | 5.0 | 5.0 | 10.0 | 10.0 |
| Z-vertex Cut Efficiency | 0.5 | 0.5 | 0.5 | 0.5 | 0.5 | 0.5 | 0.5 | 0.5 | 0.5 | 0.5 | 0.5 | 0.5 | 0.5 | 0.5 |
| Trigger Efficiency | 1.0 | 1.1 | 0.9 | 1.0 | 1.1 | 1.1 | 1.1 | 1.0 | 0.7 | 0.9 | 1.1 | 1.1 | 1.1 | 1.1 |
| Lepton ID Efficiency | 3.3 | 3.3 | 3.3 | 3.3 | 3.3 | 3.3 | 3.3 | 3.3 | 3.3 | 3.3 | 3.3 | 3.3 | 3.3 | 3.3 |
| Lepton Fake Rate | 10.4 | 6.8 | 38.1 | 43.3 | 39.9 | 24.8 | 32.8 | 34.2 | 28.8 | 34.8 | 3.1 | 5.9 | 28.1 | 26.3 |
| Jet Energy Scale | 5.5 | 0.0 | 0.0 | 3.3 | 1.6 | 1.2 | 1.6 | 0.0 | 0.0 | 1.1 | 0.1 | 0.6 | 1.8 | 1.7 |
| MC stat | 12.5 | 8.1 | 16.9 | 18.3 | 12.5 | 4.9 | 12.6 | 14.7 | 70.7 | 8.7 | 2.0 | 3.3 | 9.4 | 18.3 |
| PDF Model | - | - | - | - | - | - | - | - | - | - | 1.2 | 0.9 | 2.2 | 4.9 |
| ISR/FSR Uncertainties | - | - | - | - | - | - | - | - | - | - | 1.2 | 0.5 | 0.4 | 0.04 |

TABLE XX: Systematic uncertainties on the signal and background contributions for CDF's $WH+ZH \to jjbb$ and $VBF \to jjbb$ channels. Systematic uncertainties are listed by name; see the original references for a detailed explanation of their meaning and on how they are derived. Uncertainties with provided shape systematics are labeled with "s". Systematic uncertainties for $H$ shown in this table are obtained for $m_H = 115$ GeV/$c^2$. Uncertainties are relative, in percent, and are symmetric unless otherwise indicated. The cross section uncertainties are uncorrelated with each other (except for single top and $t\bar{t}$, which are treated as correlated). The QCD uncertainty is also uncorrelated with other channels' QCD rate uncertainties.

CDF: $WH + ZH \to jjbb$ and $VBF \to jjbb$ channel relative uncertainties (%)

| Contribution | $t\bar{t}$ | diboson | $W/Z$+Jets | VH | VBF |
|---|---|---|---|---|---|
| Jet Energy Correction | | | | 7 s | 7 s |
| PDF Modeling | | | | 2 | 2 |
| SecVtx+SecVtx | 7.6 | 7.6 | 7.6 | 7.6 | 7.6 |
| SecVtx+JetProb | 9.7 | 9.7 | 9.7 | 9.7 | 9.7 |
| Luminosity | 6 | 6 | 6 | 6 | 6 |
| ISR/FSR modeling | | | | 2 s | 3 s |
| Jet Moment | | | | s | s |
| Trigger | 4 | 4 | 4 | 4 | 4 |
| QCD Interpolation | | | | s | s |
| QCD MJJ Tuning | | | | s | s |
| QCD Jet Moment Tuning | | | | s | s |
| cross section | 10 | 6 | 50 | | |

TABLE XXI: Systematic uncertainties on the signal contributions for CDF's $H \to \gamma\gamma$ channels. Systematic uncertainties are listed by name; see the original references for a detailed explanation of their meaning and on how they are derived. Uncertainties are relative, in percent, and are symmetric unless otherwise indicated.

CDF: $H \to \gamma\gamma$ channel relative uncertainties (%)

| Channel | CC | CP | CC Conv | CP Conv |
|---|---|---|---|---|
| **Signal Uncertainties :** | | | | |
| Luminosity | 6 | 6 | 6 | 6 |
| $\sigma_{ggH}/\sigma_{VH}/\sigma_{VBF}$ | 14/7/5 | 14/7/5 | 14/7/5 | 14/7/5 |
| PDF | 2 | 2 | 2 | 2 |
| ISR | 3 | 4 | 2 | 5 |
| FSR | 3 | 4 | 2 | 5 |
| Energy Scale | 0.2 | 0.8 | 0.1 | 0.8 |
| Trigger Efficiency | – | – | 0.1 | 0.4 |
| $z$ Vertex | 0.2 | 0.2 | 0.2 | 0.2 |
| Conversion ID | – | – | 7 | 7 |
| Detector Material | 0.4 | 3.0 | 0.2 | 3.0 |
| Photon/Electron ID | 1.0 | 2.8 | 1.0 | 2.6 |
| Run Dependence | 3.0 | 2.5 | 1.5 | 2.0 |
| Data/MC Fits | 0.4 | 0.8 | 1.5 | 2.0 |
| **Background Uncertainties :** | | | | |
| Fit Function | 3.5 | 1.1 | 7.5 | 3.5 |